



## ISSUE 1/2017

### **Title Story //** **Innovation in optics and photonics**

Parameter influences on laser processing

Numerical optimization of an exhaust  
gas regulation valve

Parameter identification based on strain data

Optimization of composites in the motorcycle industry

Optimization of an electric machine

# RDO-JOURNAL

optiSLang

multiPlas

ETK

SoS



# INNOVATION IN OPTICS AND PHOTONICS – VIRTUALLAB AND OPTISLANG

Optics and Photonics play an essential role in a rising number of emerging industries. Included are all areas from everyday life to the most advanced science, e.g. light detection, telecommunication, information processing, lighting, holography, medicine, laser material processing and robotics. Highlighting the innovation potentials of optics and photonics regarding Industry 4.0, economically important applications for semiconductor photonic devices include optical data recording, fiber optic telecommunications, laser printing and optical pumping of high-power lasers. The production of modern electronic chips by lithography and wafer steppers would not be possible without optical technology. Furthermore, the car industry benefits from smart and ambient lighting. In medicine, modern optics enters more and more the operating rooms as a tool for surgery, vision correction, endoscopy and health monitoring.

In order to fulfill the challenging market requirements, a simulation driven optical system design process becomes essential. Such development processes must ensure physical optics modeling, combined with robust design optimization strategies. Here, optiSLang is the perfect companion for the leading edge optical simulation software VirtualLab Fusion. In a fully automated manner, the combination of both tools enables an efficient and reliable virtual product development of optical systems by improved design understanding, multi-objective optimization and robustness analysis. Furthermore, it is possible to perform a Robust Design Optimization, i.e. a coupled optimization and robustness analysis to obtain a design that is optimal in terms of objectives or merit functions and is robust in terms of input tolerances as well. In order to generate powerful workflows for optical systems and metamodeling, input as well as output parameters are automatically detected by optiSLang and a wizard sets up the whole workflow using the respective files exported from VirtualLab.

For some applications the integration of optics and photonics in complex systems requires the combination of optical with mechanical and thermo-mechanical modeling, e.g. by using ANSYS simulation suite. For example, this is essential for the understanding and quantification of mechanical deformation caused by thermal sources. In this challenging field of multi-physical application, optiSLang acts as an integration and automation tool to establish complex workflows with VirtualLab Fusion and other third party CAE tools.

The title story of this journal will demonstrate the interaction of VirtualLab and optiSLang to enable the optimization of a diffractive beam splitter (DBS), which divides an incident laser beam into several separated laser beams using a diffractive optical element (DOE).

Apart from that, we again have selected case studies and customer stories concerning CAE-based Robust Design Optimization (RDO) applied in different industries.

I hope you will enjoy reading our magazine.

Yours sincerely



Johannes Wiff  
Managing Director DYNARDO GmbH

Weimar, May 2017

## CONTENT

### 2 // TITLE STORY // OPTICS & PHOTONICS

Innovation in optics and photonics –  
VirtualLab and optiSLang

### 8 // CASE STUDY // OPTICS & PHOTONICS

Parameter influences on the laser processing of ceramics  
with ultra-short pulses

### 13 // CUSTOMER STORY // AUTOMOTIVE ENGINEERING

Numerical fluid optimization of an exhaust gas flap valve

### 20 // CASE STUDY // CIVIL ENGINEERING

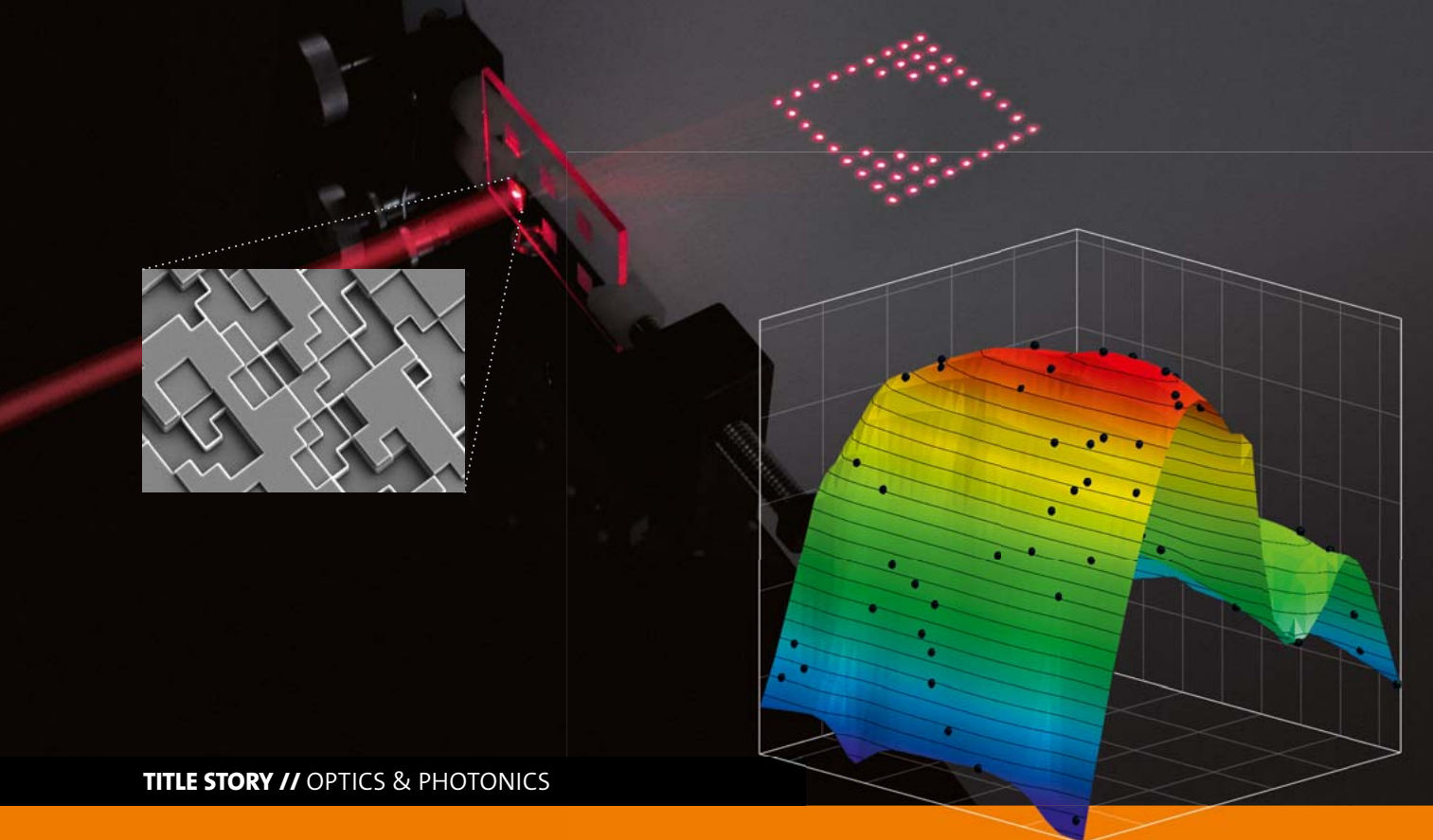
Parameter Identification based on quasi-continuous  
strain data

### 28 // CUSTOMER STORY // AUTOMOTIVE ENGINEERING

Robust optimization of continuously reinforced  
composites in the motorcycle industry

### 33 // CUSTOMER STORY // ELECTRICAL ENGINEERING

Optimization of a series production electric machine in  
shortest time



**TITLE STORY // OPTICS & PHOTONICS**

## INNOVATION IN OPTICS AND PHOTONICS – VIRTUALLAB AND OPTISLANG

**The combination of both tools enables a fast and reliable design of optical systems, design understanding, multi-objective optimization and robustness analysis in a fully automated manner.**

Light is essential for our life on earth. We see our world through light; plants and currently also humans generate energy by light and more and more technical developments need and use light to perform certain tasks. The discipline which deals with the physics and the development of devices to harness light in order to perform useful tasks is referred to as optics and photonics, although both terms are used in a somewhat redundant way.

In general, optics and photonics is understood as a technical enabler; this means it is typically an indispensable supporting part within a larger system. A laser and the optics to deliver the light to a workpiece in a fabrication robot is an example of such a combination. Virtual and mixed reality glasses and displays rely on optics but also on a lot of mechanics, electronics and computer technology. The production of modern electronic chips by lithography and wafer steppers is unthinkable without high-end optical technology as an enabling part of the fabrication process. In the car industry, smart and ambient lighting is another trend which benefits from the amazing developments in optics and photonics in recent decades. Think about the backlight illumination and the camera in a cell phone. In medicine,

not just optical microscopes, but also modern optics enters more and more the operating theatre as a tool for surgery. We would further like to mention the tremendous progress in flexible contact and intraocular lenses in the huge ophthalmic optics market. We could add numerous other examples which demonstrate the impact of optics and photonics on modern technology and our daily life. Optics is understood to be an enabling technology in the basic fields of, for example, information technology and telecommunication, healthcare and life sciences, optical sensing, lighting and energy, national defense, industrial manufacturing, and fundamental R&D.

A typical optical system consists of a technical light source or a light-emitting object, optical components which shape and control the spatial and temporal characteristics of the emitted light and components which transport the light from A to B where it is then used to perform some required effect or where it is detected to obtain information about the light-emitting object or some other sample on the way through the system. We mainly distinguish between imaging and non-imaging optical systems. An imaging system deals with providing the detector, e.g. the human eye or the



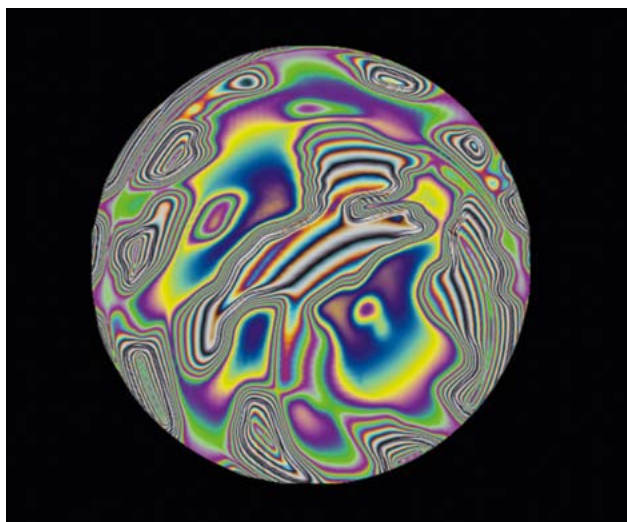


Fig. 1: The intensity of the reflected light which was obtained by multiple interference in a thin film with varying thickness. A white RGB source was applied.

sensor in a camera, with the best possible image of a self-emitting or illuminated object. In non-imaging optics, the light source is to be tailored in order to perform a specific task, e.g. the headlight of a car or the generation of a femtosecond pulse for eye surgery. Optics and photonics have benefited from various essential advances in technology in recent decades. These include the development of numerous new light sources like lasers, laser diodes and LEDs. Although optics is often understood as dealing with the visible region of the electromagnetic spectrum (only 390–700 nm), nowadays optics and photonics deal with much shorter (1 nm and below) and longer (1–10  $\mu\text{m}$ ) wavelengths as well. In the early time of optics, components were mainly restricted to planar and spherical surfaces, but nowadays we talk about freeform surfaces with aspherical, and even more general, height profiles. Optics profit from the devel-

opment of lithography for electronics, which has brought about the fields of micro- and nano-optics where surfaces are structured on a nanometer scale in order to achieve specific optical functions through the surface, or even in the volume of a bulk medium. The combination of optics with modern computer technology makes adaptive-optics concepts and detector technologies which were completely unthinkable one decade ago possible.

The new chances for innovative developments through optics and photonics have unleashed a creative demand for manipulating and controlling light in every imaginable way. The development of such innovative products requires expert tools to model and to design the optical devices in order to be able to combine the light sources, components and detectors in a way which enables the demanded function. The development of modern photonics systems cannot be done in an experimental way, but must be based on simulation technology and digital twins. For more than 2000 years, optical modeling has mainly relied on ray optics, which is often also referred to as geometrical optics. This is possible because it can be shown that the modeling and design of lens systems for imaging can, in most cases, be fully based on ray optics. However, with the development of new sources and components and the ever increasing demand for non-imaging optical functions, optical modeling and design must be based on physical optics, sometimes also referred to as wave optics, in order to provide simulation technologies which are accurate enough and which give access to all those parameters of light which are of concern for the application.

Physical optics is based on Maxwell's equations, a system of differential equations. Though mathematicians have provided powerful solvers for those equations, in optics such universal Maxwell solvers, e.g. the Finite Element Method (FEM),

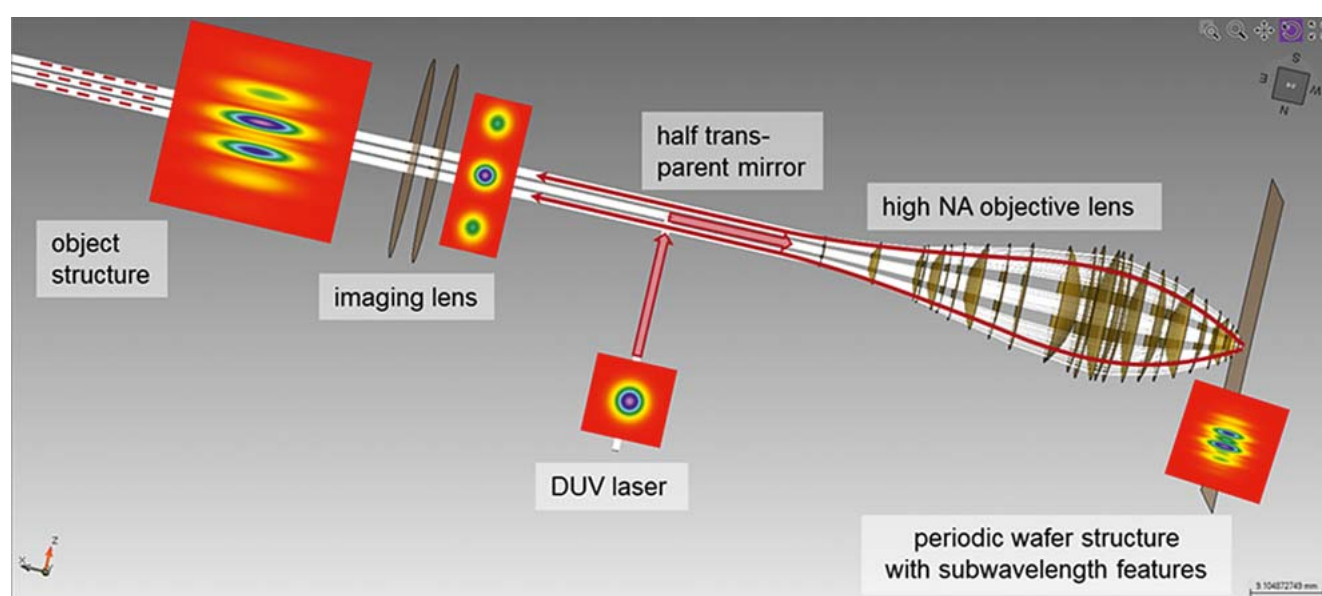


Fig. 2: Example of a complex optical setup (high-NA wafer inspection system) which often requires the application of efficient optimization tools to identify the optimum of merit functions defined by numerous different system parameters.

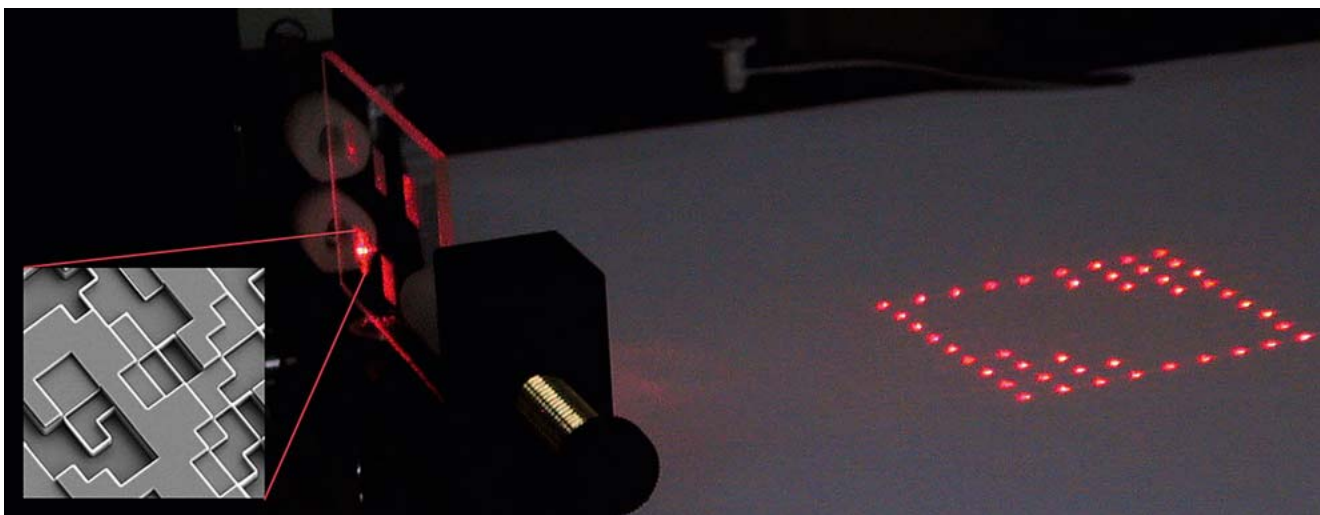


Fig. 3: Illustration of a diffractive beam splitter designed using VirtualLab and manufactured by the Institute of Applied Physics at the Friedrich Schiller University Jena – Germany

are not practical for tackling system modeling because of excessive computation time and use of computer resources. However, they are very important for modeling nano-optical devices, also as part of larger optical systems. Because of the practical limitations of these universal Maxwell solvers, ray tracing still dominates simulation technology in optics. Thus, the demand for a fast physical optics modeling concept has recently gained momentum. Prof. Frank Wyrowski and his teams at the Applied Computational Optics group at the Friedrich-Schiller-University of Jena and the companies LightTrans and Wyrowski Photonics have developed the concept of optical field tracing to provide a fast Maxwell solver which facilitates the usage of physical optics to model and design optical systems. In field tracing, different regions of a system are modeled with different specialized techniques in order to obtain a fast physical optics solution. When needed, that includes, for instance, FEM, but restricted to the smallest possible region of the system: for example the scattering sample in the modeling of a microscope. The optics software VirtualLab Fusion is based on field tracing to provide physical optics modeling and design, but includes ray tracing as well. In its second-generation field-tracing technology, which will be released in 2017, the fast physical optics concepts will be released to the public, precipitating the beginning of a breakthrough in optical modeling and design software.

The ability of fast physical optics modeling must be combined with solid concepts for the design of optical systems to perform the required optical function and to provide a system which can be fabricated with low variation of the output parameters at the same time. The design requires the optimization of the free parameters in the system, which can range from a few to hundreds and even thousands, and the analysis of the robustness of the designed system. Therefore, the Robust Design Optimization software optiSLang is the perfect companion for the optics software VirtualLab Fusion. The combination of both tools enables a fast and reliable design of optical systems, design understanding, multi-

objective optimization and robustness analysis in a fully automated manner. Furthermore, it is possible to perform a Robust Design Optimization: a coupled optimization and robustness analysis to obtain a design that is optimal and robust in terms of input tolerances at the same time. In order to enable optiSLang to realize its full power for metamodeling in optics, VirtualLab Fusion can work in a batch mode under control of optiSLang. The input parameters are defined in a dialogue in VirtualLab Fusion and the output parameters are registered by the detectors that the optical design user has defined. Both types of parameters are automatically recognized by optiSLang and a wizard is provided to set up the whole workflow using the respective files that can be exported from VirtualLab in a convenient manner. Once the workflow is established, all available analyses can be performed.

As mentioned before, optics and photonics is a technical enabler. Thus, it is always embedded in larger systems. This requires, at some stage of the Technology Readiness Level (TRL), the combination of the optical modeling with mechanical and thermomechanical modeling, e.g. with ANSYS. When the lenses of an optical system are mounted or are exposed to a thermal source, a mechanical deformation will take place that can influence the optical performance dramatically. To understand and quantify that influence, the coupling of both domains, optics and thermomechanics, is a very important but also very new and challenging field of application. There has been no software solution available that allows this coupling with VirtualLab. optiSLang acts here as an integration and automation tool to establish complex workflows with several CAx tools in order to overcome this limitation.

In the following, we want to show the combination of VirtualLab and optiSLang to enable the optimization of a diffractive beam splitter (DBS) which divides an incident laser beam into several separated laser beams using a diffractive optical element (DOE) as illustrated in Fig. 3. Important applications for such a DBS are the generation of reference patterns for motion

tracking (like Microsoft Kinect [1]) and 3D surface measurements [2], as well as the parallelization and speed increase of laser material processing [3].

The optimization of such periodic DBS microstructures is challenging if large diffraction angles need to be realized. This kind of high-numerical-aperture (NA) DBSs must have microstructured features in the order of the wavelength of light. This requires a fully vectorial and rigorous analysis of the light interaction with the microstructure, which is beyond the scope of the typically applied thin-element approximation (TEA) [4]. For example, the high-NA DBS given in Fig. 4 will be optimized by a combination of VirtualLab's Fourier Modal Method [5] (which is a rigorous and fully vectorial solver of Maxwell's equations) and optiSLang.

As optimization target, the total diffraction efficiency  $\eta$

$$\eta = \eta_1 + \eta_{-1} + \eta_3 + \eta_{-3} + \eta_5 + \eta_{-5}$$

should be maximized and the uniformity error  $U$  should be

$$U = \frac{\eta_{\max} - \eta_{\min}}{\eta_{\max} + \eta_{\min}} < 0.5\%$$

Here,  $\eta_i$  with  $i \in \{-5; -3; -1; +1; +3; +5\}$  represent the diffraction order efficiencies of the 6 beams to be generated by the DBS. In addition, due to fabrication constraints, the smallest feature size of the microstructure should be larger than 300nm. The free parameters which should be optimized by the parametric optimization are the lengths of the 6 intervals (L1-L6) within one DBS structure period given in Fig. 5. Furthermore, the scaling of the modulation depth (z-Scaling) is a free parameter. An initial design result was obtained by VirtualLab's Iterative Fourier Transformation Algorithm. In the following, this design should be further improved performing, at first, a sensitivity analysis, followed by a parametric optimization.

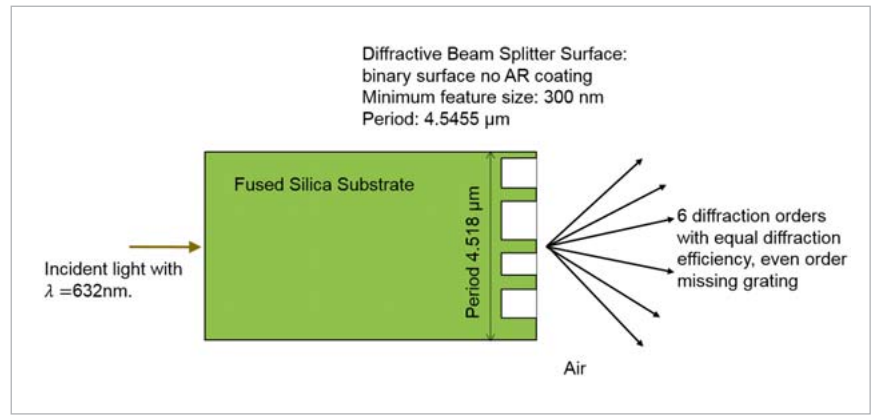


Fig. 4: High-NA DBS setup dividing one incident beam into 6 beams with the same diffraction efficiency. This setup will be optimized in the following by a combination of VirtualLab Fusion and optiSLang.

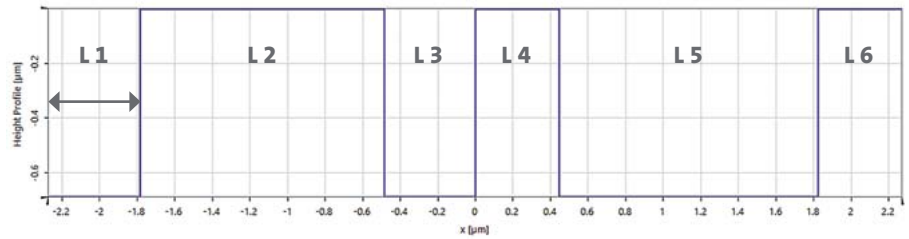


Fig. 5: Cross-section along a single period of the DBS microstructure. The structure is parametrized by the width of the six intervals. In addition, there is a free height scaling factor to adjust the profile height.

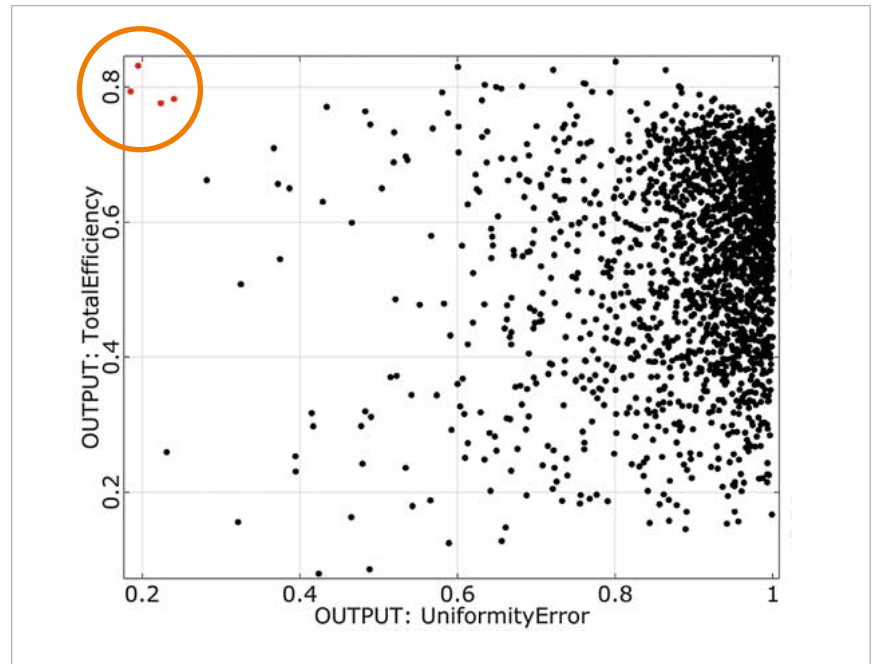


Fig. 6: Results I of the sensitivity analysis performed by optiSLang. The objective is in a small subspace: only 4 out of 2000 samples are close to the optimum.

In a first step, a sensitivity analysis is done in optiSLang to identify the optimization potential by estimation of the variation of response. This sensitivity analysis also helps to understand and verify dependencies between input and response variations using metamodels. An advanced Latin hypercube sampling was used to scan the parameter space using 2000 different DBS designs. The performance of these 2000 designs is shown in Fig. 6.



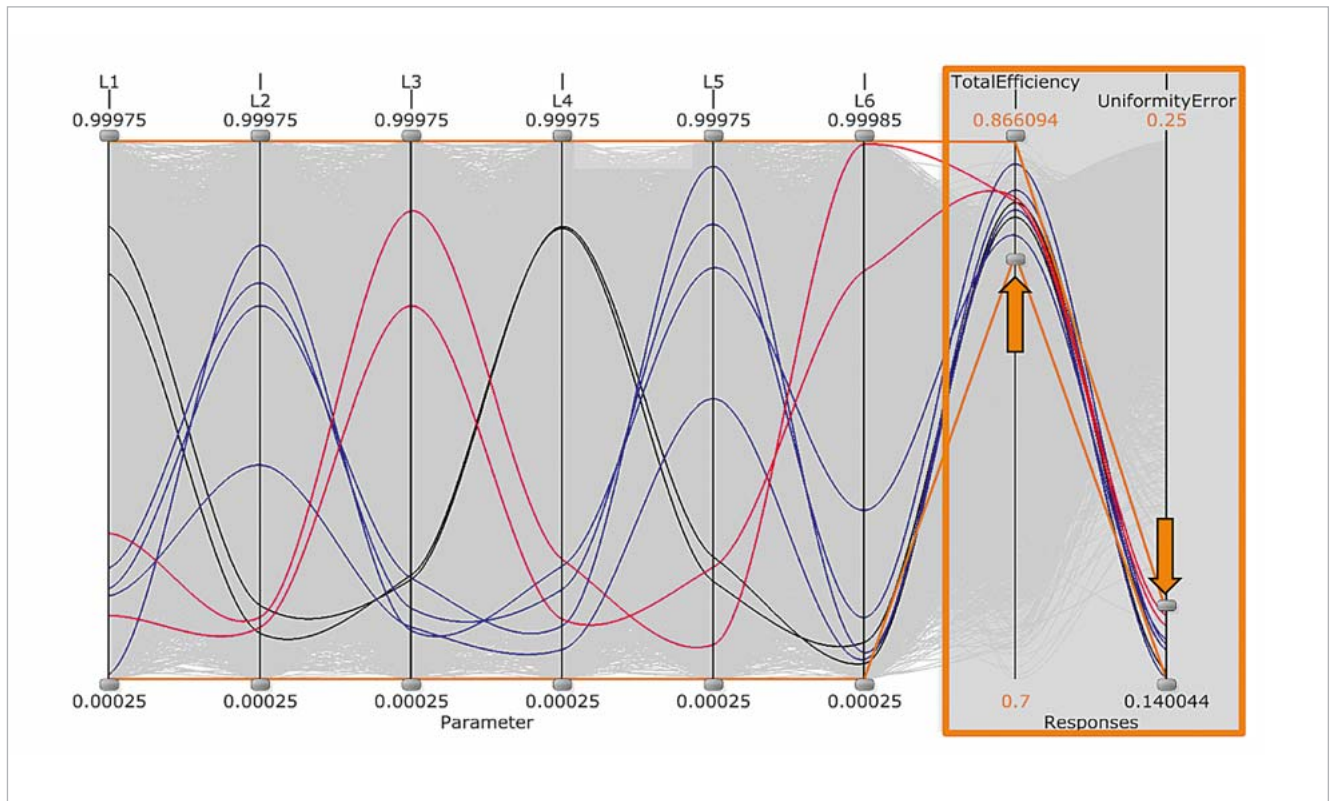


Fig. 7: Results II of the sensitivity analysis performed by optiSLang. Corresponding widths L1/L4, L2/L5 and L3/L6

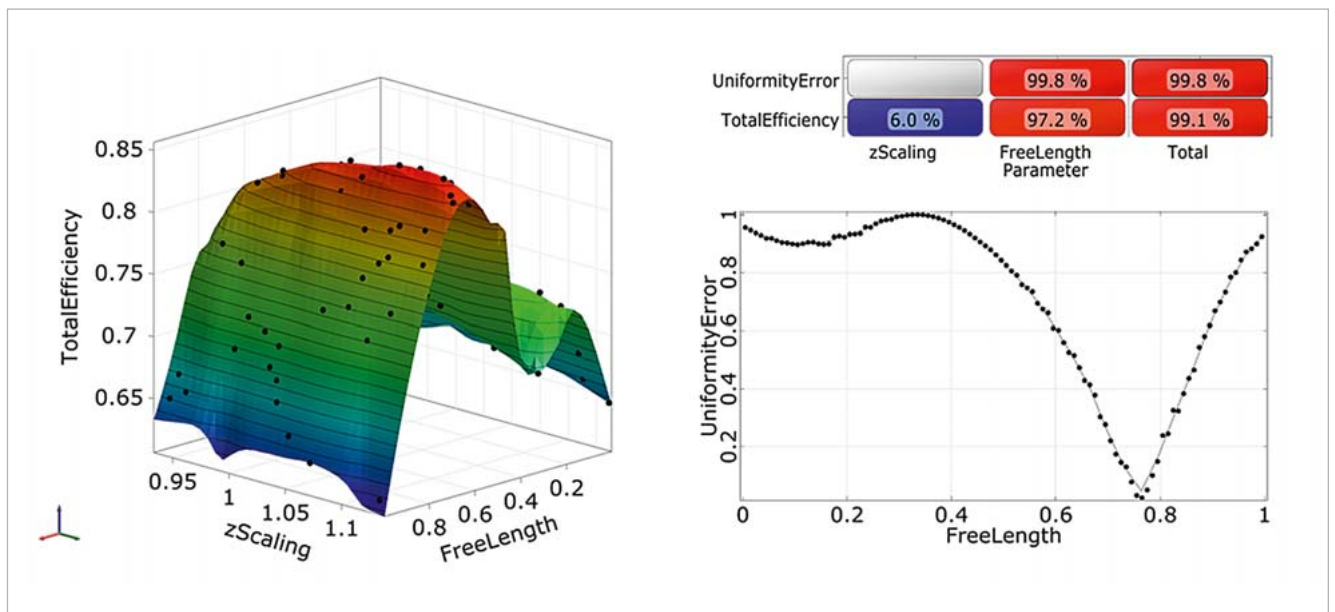


Fig. 8: Results III of the sensitivity analysis performed by optiSLang. A metamodel is found describing the response of the design (COP>99%). All responses depend strongly on the FreeLength parameter. The Uniformity Error is independent of z-Scaling within the chosen parameter range.

Designs exist where both objectives are not, or are only slightly, in conflict. Consequently, the definition in one objective function or with uniformity error  $U$  as a constraint will be most efficient. The parallel coordinate plot given in Fig. 7, which is another result of the sensitivity analysis, indicates that for designs close to the optimum ( $U < 25\%$ ,  $> 70\%$ ), the lengths L1/L4, L2/L5 and L3/L6 correspond to each other.

Consequently, we can assume  $L2=L5$  and  $L1=L3=L4=L6$  (due to the periodicity of the microstructure). Thus, we can reduce the number of free parameters describing the widths of the intervals to a single free parameter, which is called FreeLength in the following. As shown in Fig. 8, the newly introduced FreeLength parameter has significant influence in the DBS performance. The z-Scaling parameter has just a minor influence.



After reducing the complexity of the optimization problem from 7 to 2 free parameters, a parametric optimization based on the Adaptive Response Surface Method (ARSM) by optiSLang is performed. The optimization results are shown in Fig. 9. The uniformity error could especially be reduced significantly.

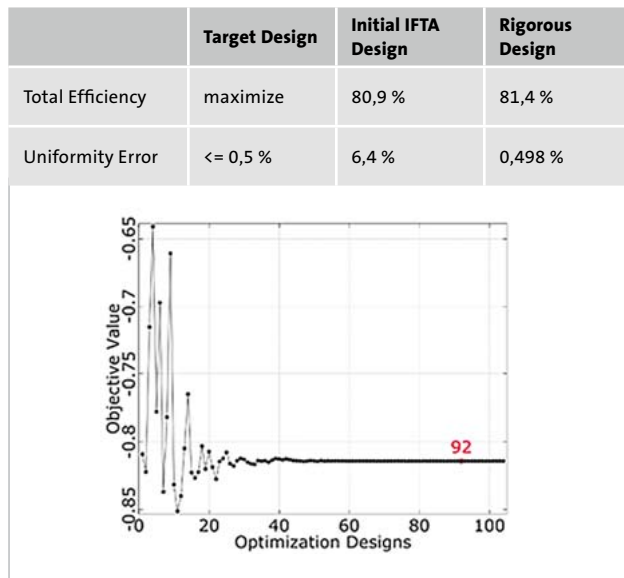


Fig. 9: Rigorous parametric optimization of DBS using optiSLang's ARSM. The uniformity error could especially be significantly lowered by the rigorous parametric optimization design.

It is evident that optics and photonics have a vital role to play in the current framework of technological innovation, both in its own right and as an enabler for other fields. The ever more stringent requirements increasingly imposed on optical systems in order to realize the ever more imaginative applications coming into vogue can no longer be met satisfactorily with bare-bones ray tracing: there is, consequently, a tendency towards simulation paradigms able to incorporate the full physical-optics picture within realistic constraints of simulation time and computation requirements. And this is precisely the answer that VirtualLab Fusion provides with its second-generation field-tracing approach.

But technological and scientific innovation seldom takes place within the closed confines of a single subject matter: bringing together expertise from different fields is what, throughout history, has tended to yield the best results. This is the backdrop for the collaboration between VirtualLab Fusion and optiSLang. Combining the paradigm-shifting field-tracing concept of VirtualLab Fusion with the cutting-edge optimization skills of optiSLang will open the door to a new level in the realm of optical system design.

#### Authors //

Roberto Knoth, Stefan Steiner, Christian Hellmann, Olga Baladron-Zorita (LightTrans International UG) / Frank Wyrowski (Friedrich Schiller University Jena)

Source // [www.dynardo.de/en/library](http://www.dynardo.de/en/library)

#### References //

1. Du, Pei-Qin, SHIH, Hsi-Fu, CHEN, Jenq-Shyong y WANG, Yi-Shiang. "Design and verification of diffractive optical elements for speckle generation of 3-D range sensors". *Optical Review*. 2016, vol 23, 6, p. 1017–1025.
2. Chan, Shih-Yu, Hsi-Fu Shih, Jenq-Shyong Chen. "Depth measurement using structured light and spatial frequency". *Appl. Opt.* 2016, vol 55, 19, p. 5069–5075.
3. Taghizadeh, M.R., P. Blair, K. Ballüder, A.J. Waddie, P. Rudman, N. Ross. "Design and fabrication of diffractive elements for laser material processing applications". *Optics and Lasers in Engineering*. 2000, vol 34, 4–6, p. 289 - 307.
4. Wyrowski, F. & Kuhn, M. (2011), "Introduction to field tracing", *Journal of Modern Optics* 58(5-6), p. 449-466.
5. Li, Lifeng. *Mathematical Reflections on the Fourier Modal Method in Grating Theory*. Philadelphia, PA, USA: Society for Industrial and Applied Mathematics, 2001, p. 111–139.



## TRAINING

### Webinars and Info Days

At our webinars, you will receive an introduction to performing CAE-based optimizations and stochastic analyses. During an information day, you will additionally have the opportunity to discuss your specific optimization task with our experts.

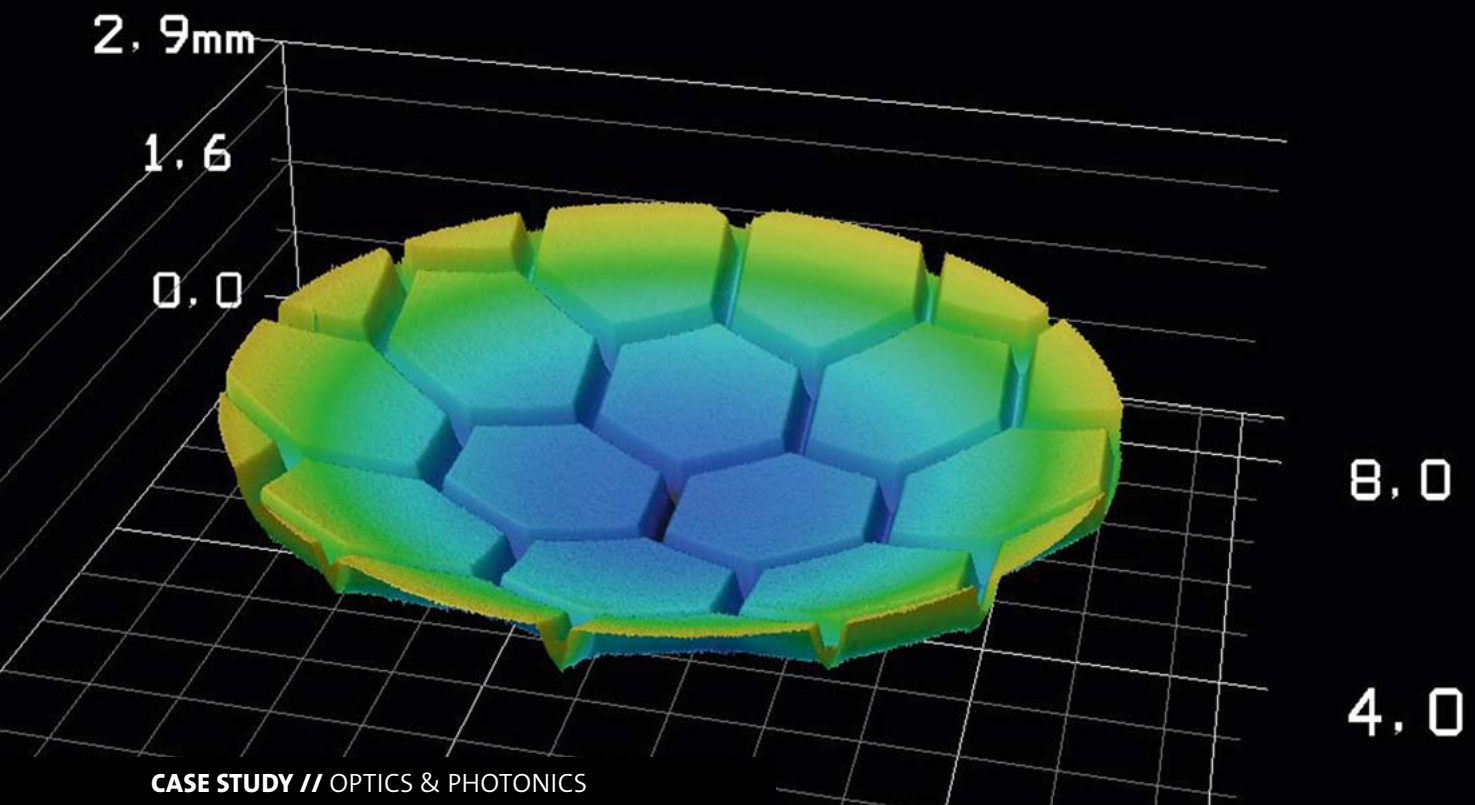
### Training

For a competent and customized introduction to our software products, visit our basic or expert training clearly explaining theory and application of a sensitivity analysis, multidisciplinary optimization and robustness evaluation.

### Info

You will find all information and the current training program at:

[www.dynardo.de/en/training](http://www.dynardo.de/en/training)



## PARAMETER INFLUENCES ON THE LASER PROCESSING OF CERAMICS WITH ULTRA-SHORT PULSES

Within the scope of a sensitivity analysis, optiSLang is used to investigate the main influencing variables in complex laser material processing. With the help of real laboratory data, physical correlations can be revealed and examined.

### Introduction

High-performance ceramics such as alumina have been firmly established for the manufacturing of tools and components in the modern electronics industry and mechatronics. Various components, for instance circuit boards, bearings and sensors, benefit from specific characteristics, such as wear resistance, stiffness and electrical neutrality. Nevertheless, the mechanical processing of ceramics is often a difficult task. For this reason, modern laser technologies, which enable a contactless and wear-free processing, have been used to process ceramics for some time now, for instance for cutting, scribing or drilling.

However, regarding high-precision applications such as surface functionalization, micro-drilling or three-dimensional structuring, conventional laser processes reach their limits. Especially due to the thermal influences of the laser radiation, brittle edges, stresses and redeposited layers emerge. Ultra-short pulse lasers, which have been industrially available for a few years, allow for completely new surface qualities. The extremely short pulse durations in the pico- and femtosecond range lead to non-linear absorption mechanisms and an almost athermal material removal. Even brittle-hard, dielectric substrates can be processed precisely and gently.

Nevertheless, many questions regarding the ablation mechanisms and the beam-material-interactions of ceramics and ultra-short pulses still have not been entirely clarified. As shown in Fig. 1, the material removal with ultra-short pulses is an extremely complex process, which is influenced by a variety of parameters. Besides the material properties and the environmental conditions, the laser parameters such as wavelength, pulse duration and repetition rate predominantly influence the process. The pulsed radiation can be characterized by different energy-related variables, such as pulse energy, average power, or energy density, which is referred to as fluence. It often remains uncertain which of these factors describes the process best. Moreover, the parameter field is complemented by the process variables, which are defined by the scanner movement leading to a two-dimensional surface ablation. While the pulse distance within a scan line results from the marking speed, the distance between the scan lines is freely selectable.

In order to reveal and optimize the processes happening during surface ablation, investigations on alumina ( $\text{Al}_2\text{O}_3$ ) have been executed. The particular aim was to examine a

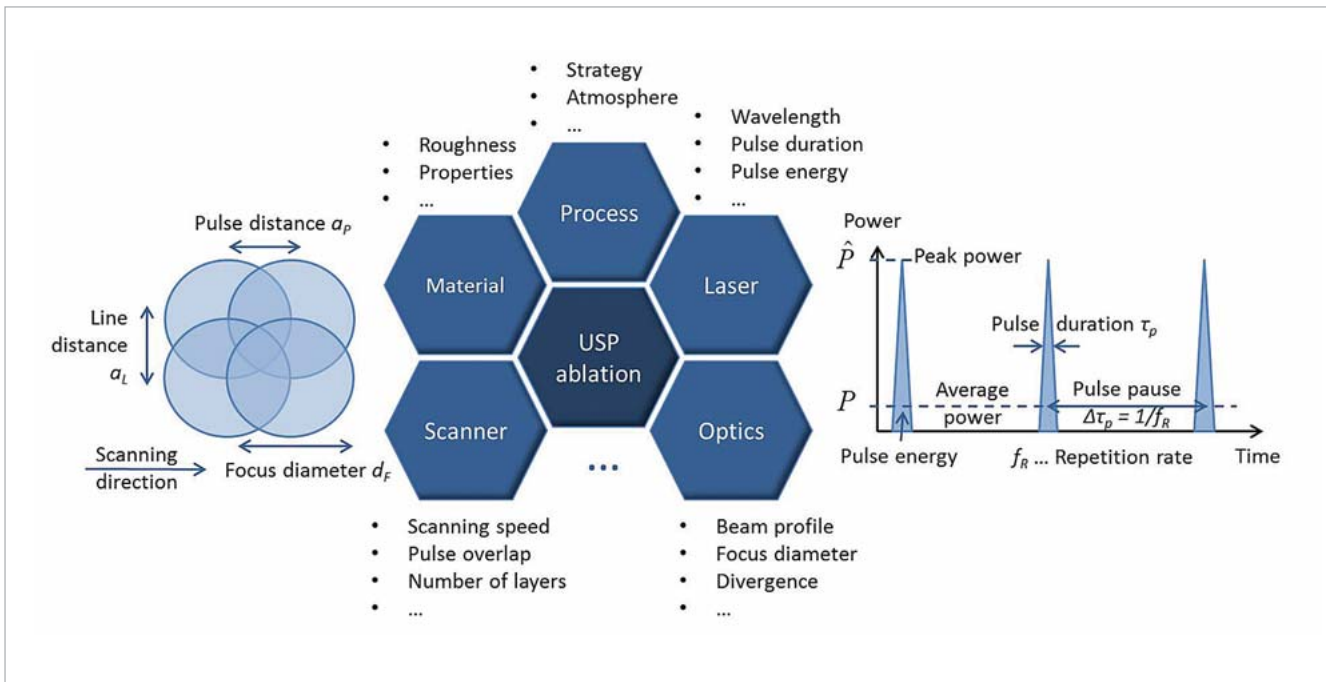


Fig. 1: The ultra-short pulse ablation is influenced by a multitude of parameters

large number of parameters simultaneously regarding their influences on the ablation process as well as their interactions among each other. For this purpose, optiSLang was used to execute a Design of Experiments as part of a sensitivity analysis.

### Experimental Approach

The experiments were carried out with a mode-coupled solid state laser (Lumera Laser, Hyper Rapid 25) with a pulse duration of 9 ps and a wavelength of 1064 nm. Via external frequency conversion, the second and third harmonic are generated so that two other wavelengths, 532 nm and 355 nm, are available. The beam, which has a Gaussian shaped intensity profile, is deflected by a galvo scanner and focused with f-theta objectives of varying focal lengths.

Using the Latin Hypercube sampling, an experimental design with 100 parameter combinations was set up. These have been applied to fields of 5 mm x 5 mm filled with parallel scanning lines to remove the material within the entire area. The evaluation of the ablation process is based on the output parameters of profile depth and roughness. These have been measured with the aid of a laser scanning microscope (Keyence, VK-X100). The roughness was determined by a multiple line scan and the profile depth by measuring the step distance between initial and processed surface (Fig. 2). To evaluate the efficiency of the process, the ablation rate was calculated as the ratio of ablated volume and processing time. Furthermore, the ablation per layer has been determined as the ratio of profile depth and number of layers. This output parameter provides information on how uniformly the removal process continues into depth.

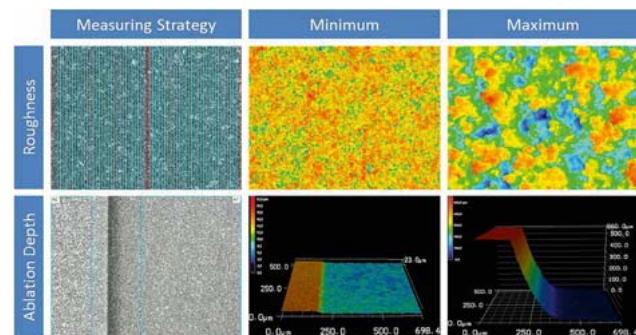


Fig. 2: Measurement of the main responses – roughness and ablation depth

Table 1 (see next page) gives an overview of the input and output parameters. While some inputs can be changed directly by the machine settings, others result from physical connections (controlled variables). Concerning the sensitivity analysis, all listed parameters have been taken into account to identify their significance for the removal process. For this purpose, the external data measured in the laboratory have been imported to optiSLang using the Excel Add-in and analyzed with the help of the Metamodel of Optimal Prognosis (MOP).

### Sensitivity Analysis

In addition to the one-dimensional sensitivity analysis using the extended correlation matrix, the coefficient of prognosis (COP) has especially been used to analyze the data within a multidimensional sensitivity analysis. Considering all input parameters, it is found that the roughness is in particular dependent on fluence and pulse overlap, whereas the output parameters connected with the ab-

Input Parameters				Output Parameters	
actuating variables		controlled variables			
Power $P$ [W]	0.3 ... 20	Fluence $F$ [J/cm <sup>2</sup> ]	0.1 ... 32	Roughness $R_a$ [ $\mu$ m]	0.42 ... 3.8
Wavelength $\lambda$ [nm]	355; 532; 1064	Pulse distance $a_p$ [ $\mu$ m]	1 ... 15	Ablation rate $A$ [mm <sup>3</sup> /s]	0 ... 7.8
Scanning speed $v_s$ [mm/s]	200 ... 3000	Horizontal Overlap $O_h$ [%]	-33 ... 99	Ablation depth $t$ [ $\mu$ m]	0.24 ... 543
Line distance $a_l$ [ $\mu$ m]	1 ... 15	Vertical Overlap $O_v$ [%]	-33 ... 99	Ablation/layer $ApL$ [ $\mu$ m]	0.018 ... 31.5
Focal length $f$ [mm]	40; 80; 100; 250	Focus diameter $d_f$ [ $\mu$ m]	12 ... 100		
Number of layers $N$	1 ... 20				

Table 1: Overview of input and output parameters with associated value ranges

lation depth can be better explained by power as well as pulse and line distance. This shows that the focus diameter, which is required for the calculation of fluence and overlap, especially has a significant influence on the quality of the processed surface.

Due to the physical relation of the input parameters, high input correlations occur, which reduce the model quality and make realistic conclusions difficult. For this reason, it is necessary to filter the parameters in such a way that input correlations are avoided and physically meaningful models of high prognosis ability are generated. By filtering power, focus diameter as well as pulse and line distance, a metamodel could be created that explains roughness-related phenomena very well. However, since the design of experiments has been set up with precisely these parameters, only small COPs are achieved due to an asymmetric distribution of the experimental points. By contrast, high COPs occur by removing the calculated variables of fluence and pulse overlap. This model (Fig. 3) is of particular impor-

tance for the explanation of phenomena associated with the depth parameters. In order to investigate the processes leading to ultra-short pulse ablation of ceramics, both models have been considered, though. The essential findings are summarized in the following.

### Optimization of roughness

In the majority of cases, the roughness rises if power (or fluence) and pulse overlap are increased. However, the metamodeling indicates that there exists an optimal pulse distance and therefore an optimal pulse overlap, for which the roughness can be reduced. Starting from this point, the roughness rises for both increasing and decreasing overlap.

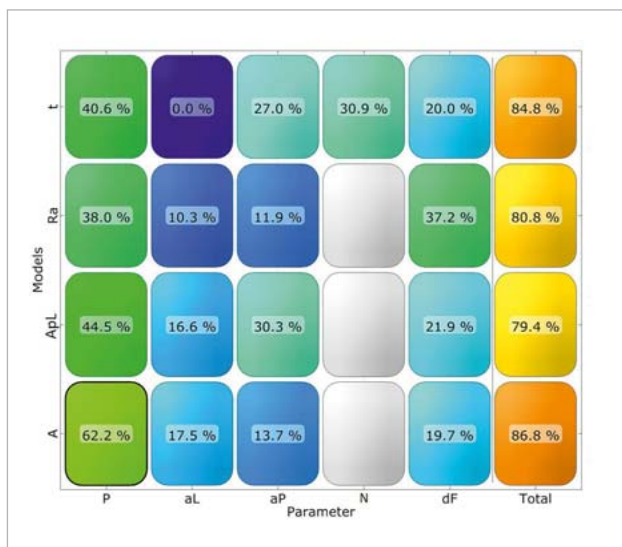


Fig. 3: COP-matrix of best meta-model

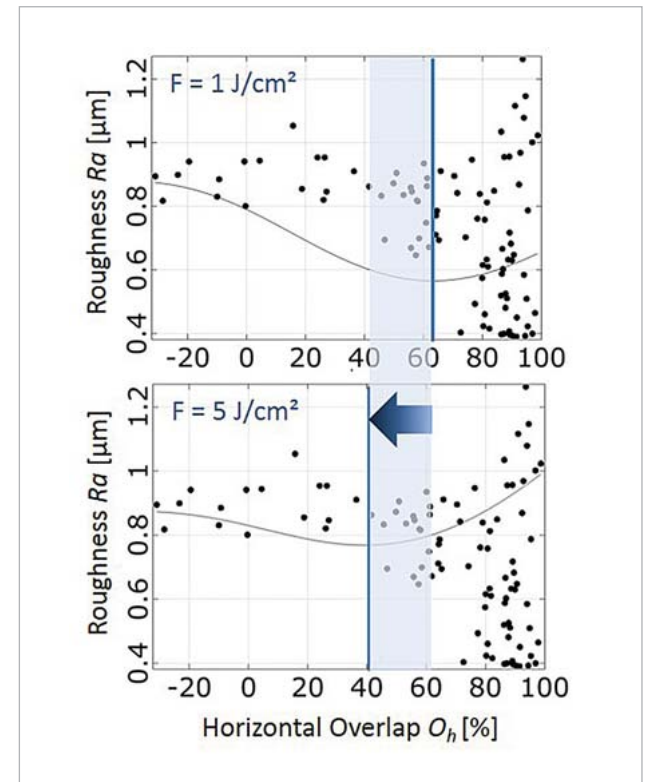


Fig. 4: Fluence dependent shifting of pulse overlap to minimize roughness



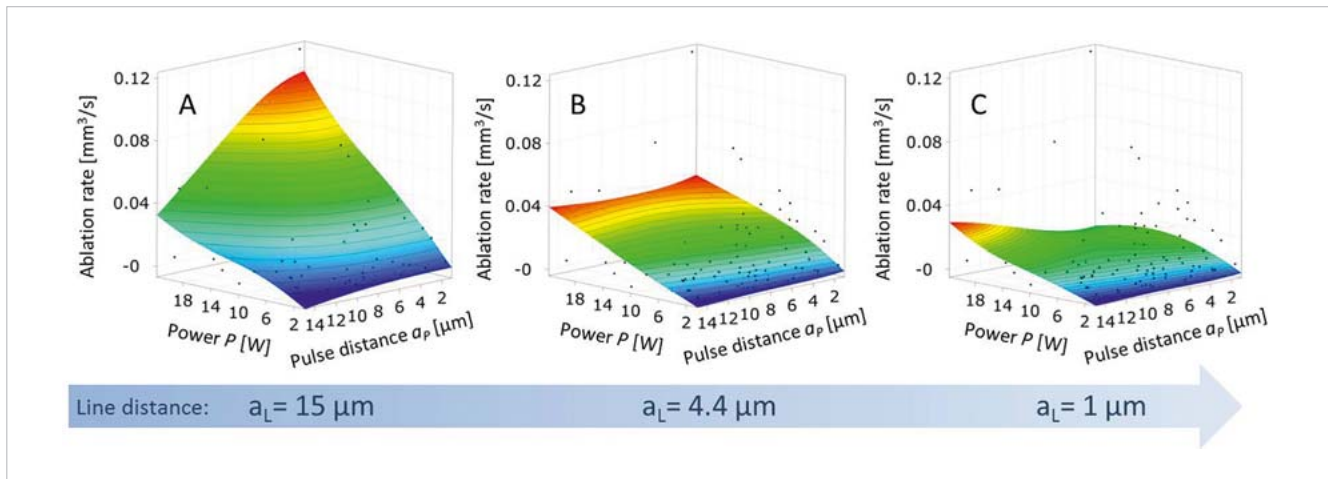


Fig. 5: Ablation rate in dependence of pulse distance and line distance

This optimum strongly depends on the energy density. As can be seen in Fig. 4, the pulse overlap leading to a minimal roughness shifts to smaller values if the fluence is increased. This observation can be explained by the fact that the effective ablation diameter increases with an increase of power which leads to a larger effective overlap. As a result, good surface qualities are achievable even for high fluences, just by adapting the pulse distance.

#### Optimization of ablation rate

The depth-related output parameters mainly depend on the average laser power. Fig. 5 shows that the ablation rate rises steadily with an increase of power. In addition, the pulse distance as well as the line distance have a decisive influence on the effectiveness of the material removal. The response-surface-diagrams reveal that the functional relation between ablation rate and pulse distance significantly changes through a variation of the line distance.

In the case of large line distances (Fig. 5A), the removal rate increases with decreasing pulse distance. This is due to the increasing pulse overlap, which generates higher ablation depths. The high influence of the pulse distance on the ablation depth can also be seen in the COP matrix (Fig. 3). In addition to the ablation depth, the ablation rate is also determined by the processing speed. Since small pulse distances are generated by the use of low scanning speeds, they generally have a negative effect on the removal rate. However, the steady increase of the ablation rate with decreasing pulse distance shows that this effect only plays a subordinate role.

On the other hand, regarding small line distances (Fig. 5C), a completely different functional interrelationship between ablation rate and pulse distance can be observed. Especially at high power, the removal rate now rises with increasing pulse distance, i.e. with decreasing pulse overlap. This seems to contradict the previous observations, but can be justified by the high influence of the line distance

on the ablation rate. It has a considerably higher impact on the process efficiency than the scanning speed. Decreasing line distances, as well as small pulse distances, generates higher pulse overlaps and thus leads to an increase of the removal depth. However, small line distances also mean that the area to be processed has to be filled with more scanning lines. Due to the many jumping and marking vectors to be executed, the processing time increases significantly. For this reason, the ablation rate generally decreases with decreasing line distance. The loss of time at small line distances is so crucial that the scanning speed gains in importance. High marking speeds and resulting high pulse distances can now lead to an increase of the ablation rate.

In between exists a line distance for which the opposing influences of the pulse distance on the ablation depth and the processing time compensate for each other so that an independence of the removal rate from the pulse distance can be detected (Fig. 5B).

#### Optimization of ablation depth

In addition to the surface quality described by the roughness and the process efficiency described by the ablation rate, it also makes sense to take a closer look at the parameter dependencies for the actual material removal indicated by the ablation depth and the ablation per layer. According to the COP matrix, the number of layers is the second most important influencing factor for the ablation depth, only surpassed by the laser power. This is easy to understand and just what was to be expected. Much more interesting is the fact that the number of layers has no influence on the remaining responses at all. This indicates that the ablation process continues constantly into depth. Each layer can be processed under the same conditions, irrespective of the number of layers which have already been removed. Such a behavior is a prerequisite for the three-dimensional structuring of the material with high shape accuracy. As a result, a high agreement of calculated target contours with processed actual contours can be ensured.

## Summary and Discussion

Within the scope of the investigations, it was shown that optiSLang can be used to create reliable and physically meaningful metamodels based on experimental data. These can be used for the identification and analysis of complex laser processes as well as for their optimization. It should be noted, however, that the models must always be thoroughly examined regarding their validity. In particular, a filtering of input parameters has to be executed in order to avoid input correlations and to obtain well-founded models. Moreover, the collection of experimental data always requires a special degree of carefulness since both the adjustment of the input parameters and the recording of the responses are subject to process and measurement fluctuations.

Especially in the context of investigating the beam-material-interactions and the ablation process of alumina with the aid of optiSLang, useful new insights into the ultra-short pulse laser ablation of technical ceramics could be gained. The results concerning the surface quality show that it is possible to achieve acceptable roughness values even at high laser powers by optimizing the pulse overlap. These are sufficient for at least most possible applications. In this case, the general rule of laser materials processing that quality and quantity cannot be reconciled. It can at least be somewhat softened. Regarding the efficiency of the process, it could be shown that it makes sense to consider pulse distance and line distance separately in order to generate the highest possible ablation rates. This contradicts the so far existing strategy of always equating pulse distance and line distance in favor of a homogeneous energy distribution.

All in all, it can be summarized that, in addition to the parameter optimization, optiSLang can be used to gain significant new insights into physical processes. For this rea-

son, further experiments regarding the ultra-short pulse ablation of technical ceramics will be carried out. Due to the technical characteristics of the machinery such as the availability of varying power ranges for different wavelengths, an asymmetrical design space has been used thus far. This allowed the involvement of a broad value range, but has shown a negative effect on the model quality, characterized by reduced COP values. For further investigations, the experimental design has to be changed to validate the collected findings and to increase the model quality. Including further technical ceramics, the influence of the material shall be examined in order to gain an even better understanding of ultra-short laser processes.

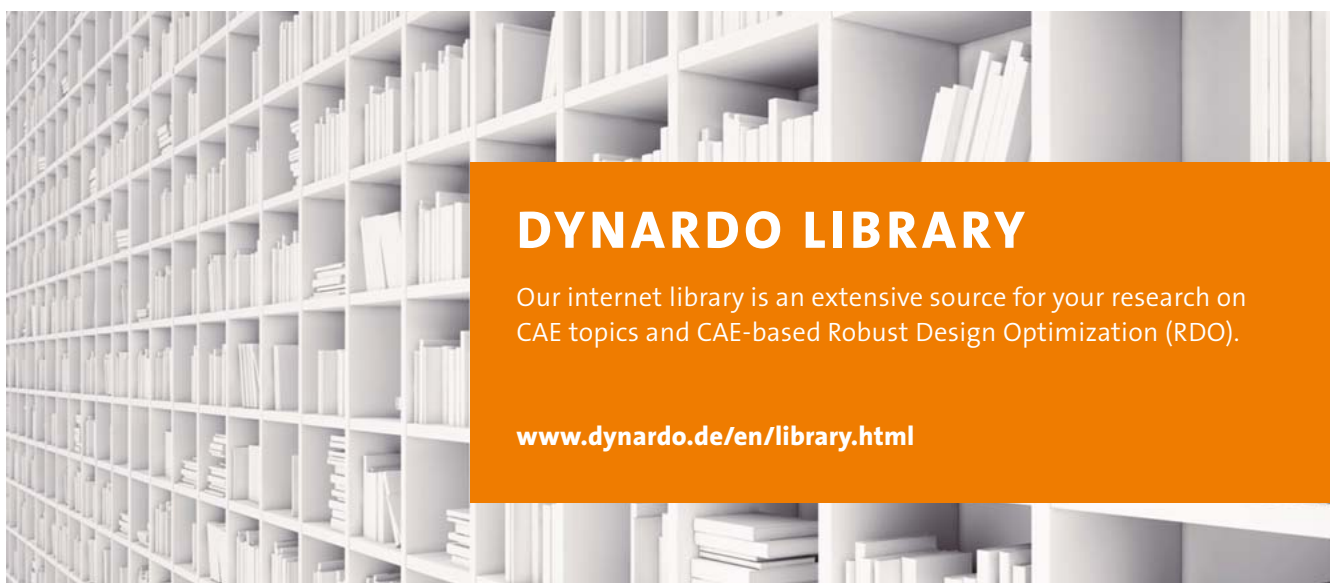
### Author //

Maria Friedrich (ifw - Günter-Köhler-Institut für Fügetechnik und Werkstoffprüfung GmbH) / Kristina Völlm, Jens Bliedtner (Ernst-Abbe-Hochschule Jena)

### Source //

[www.dynardo.de/en/library](http://www.dynardo.de/en/library)

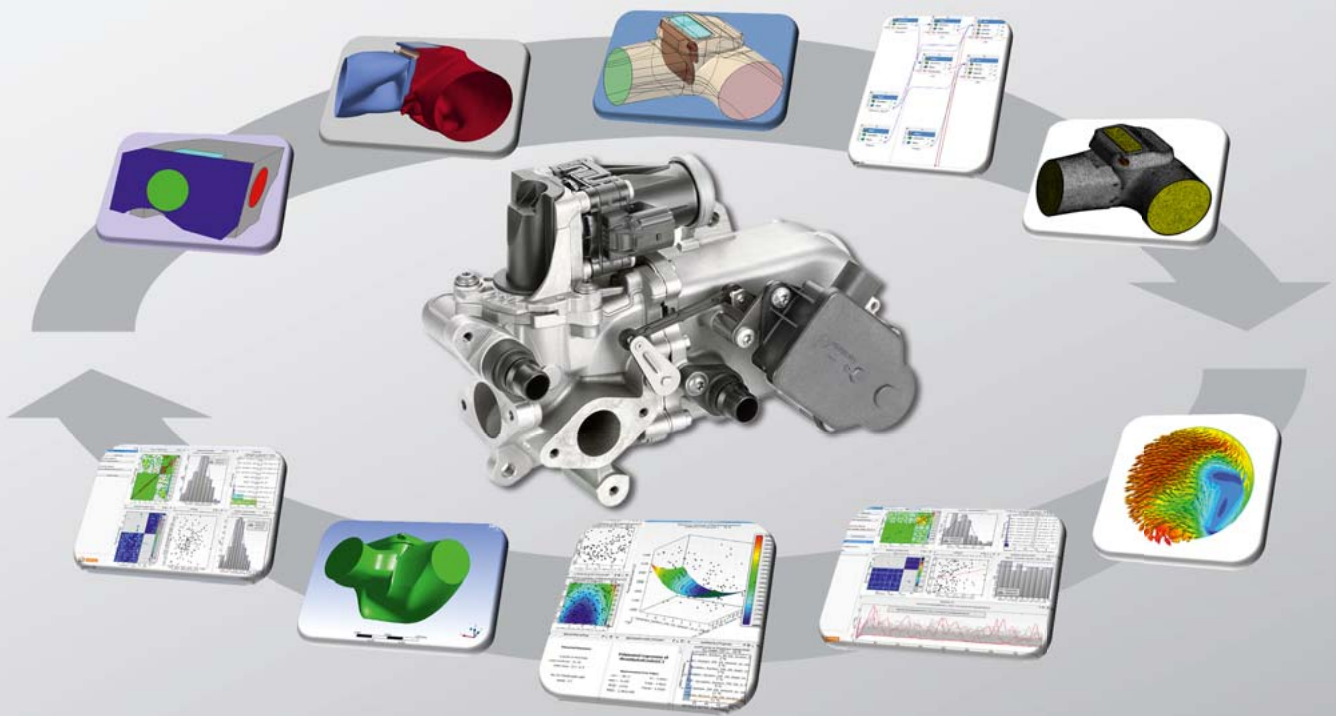
The presented results have been obtained in a research project (2015 VF0021) which is supported by the free state of Thuringia. A cofinancing is carried out by the Europäischer Fonds für regionale Entwicklung (EFRE). This support is gratefully acknowledged.

## DYNARDO LIBRARY

Our internet library is an extensive source for your research on CAE topics and CAE-based Robust Design Optimization (RDO).

[www.dynardo.de/en/library.html](http://www.dynardo.de/en/library.html)



## CUSTOMER STORY // AUTOMOTIVE ENGINEERING

# NUMERICAL FLUID OPTIMIZATION OF AN EXHAUST GAS FLAP VALVE

From topology optimization results for the valve flow channel, a parametric CAD model is generated for a parameter-based optimization and robustness analysis.

## Introduction

In recent years, the reduction of pollutant emissions has become a significant issue for environmental policy, not only because of the latest emission scandals. Consequently, the reduction of pollutant emissions is an eminently important factor in the development of fuel engines. One of the most decisive factors for the reduction of pollutants is the exhaust gas recirculation (EGR). The principle of recirculation ensures that the exhaust gas is partially resupplied to the incoming fresh air, resulting in a reduction of nitrogen oxide emission. Here, an optimized geometry regarding flow-technical aspects essentially ensures a lower pressure loss and a consistent fluid flow.

## EGR-process & optimization goal

In this study, optimization objectives for EGR flap valve have been focusing on fluid mechanical characteristics at two load cases for the following reasons:

1. At full load (EGR valve is closed), the lowest possible pressure loss in the entire exhaust gas system is aspired to achieve low fuel consumption of the combustion engine.
2. At partial load (EGR valve is opened; Fig.1), a low-loss in-

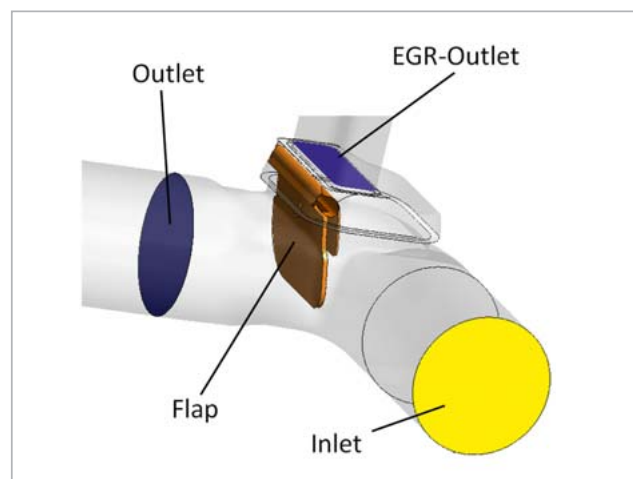


Fig. 1: Flow chamber of an EGR valve

flow into the EGR passage is desired in order to ensure a small scavenging gradient and low throttling to reach the required EGR rate. Additionally, uniform mass flow distribution is required upstream of the EGR cooler in order to ensure high cooling efficiency which is advantageous regarding fuel efficiency of the engine as well.

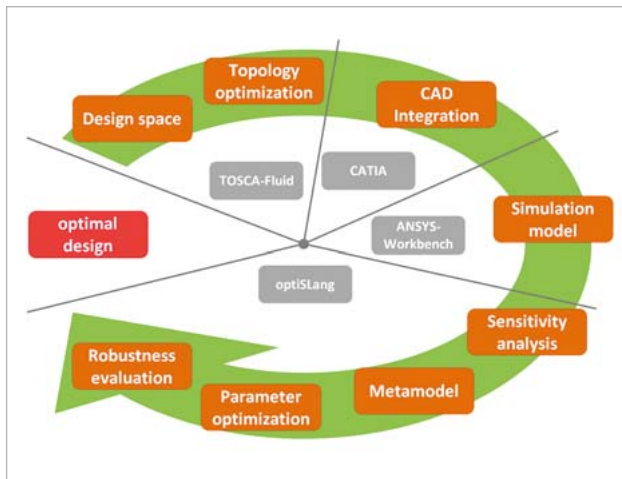


Fig. 2: Optimization workflow

Thus, the objective function includes the reduction of the pressure loss at full load as well as the uniformity of flow towards the EGR cooler in the partial load case.

### Frontloading & optimization workflow

The optimization workflow (Fig. 2) is applied at an early project state in order to reduce product development time, to improve technical product quality and to consider maximum innovation potential at the same time. In this context, it is necessary to support the design team already in the offering phase in order to realize active frontloading. For this purpose, a topol-

ogy optimization of the flow channel is executed for the maximum available design space by the use of Simulia Tosca Fluid. The result is a first conceptual and highly innovative design for both load cases. In the next step, both designs are converted into a parametric Dassault CATIA V5 CAD model which takes manufacturing constraints into account. The implementation of manufacturing constraints and a strong collaboration with the design team during the CAD parameterization ensures meaningful parametric optimization results and reduces the effort in transferring the optimized geometry into the detailed design. By varying the CAD parameters, resulting geometries from topology optimization for both load cases as well as further design states can be represented. The CAE workflow automation and simulation model setup for parametric CAD geometry is defined by the use of ANSYS Workbench. Afterwards, the ANSYS Workbench project is linked to the process steering and optimization software optiSLang. Reasonably, numerical DoE and sensitivity analysis are executed as initial steps in order to explore the entire design space and to build up a database for metamodeling. The sensitivity analysis in particular provides better understanding of complex technical systems and, therefore, adds considerable value to the product know-how. As aforementioned, the resulting database is used to create numerical metamodels which can be referred to optimization algorithms in order to reduce the required amount of CAE solver runs. A minimized optimization objective in combination with a parametric CAD model yields to a design which covers improved flow characteristics for both

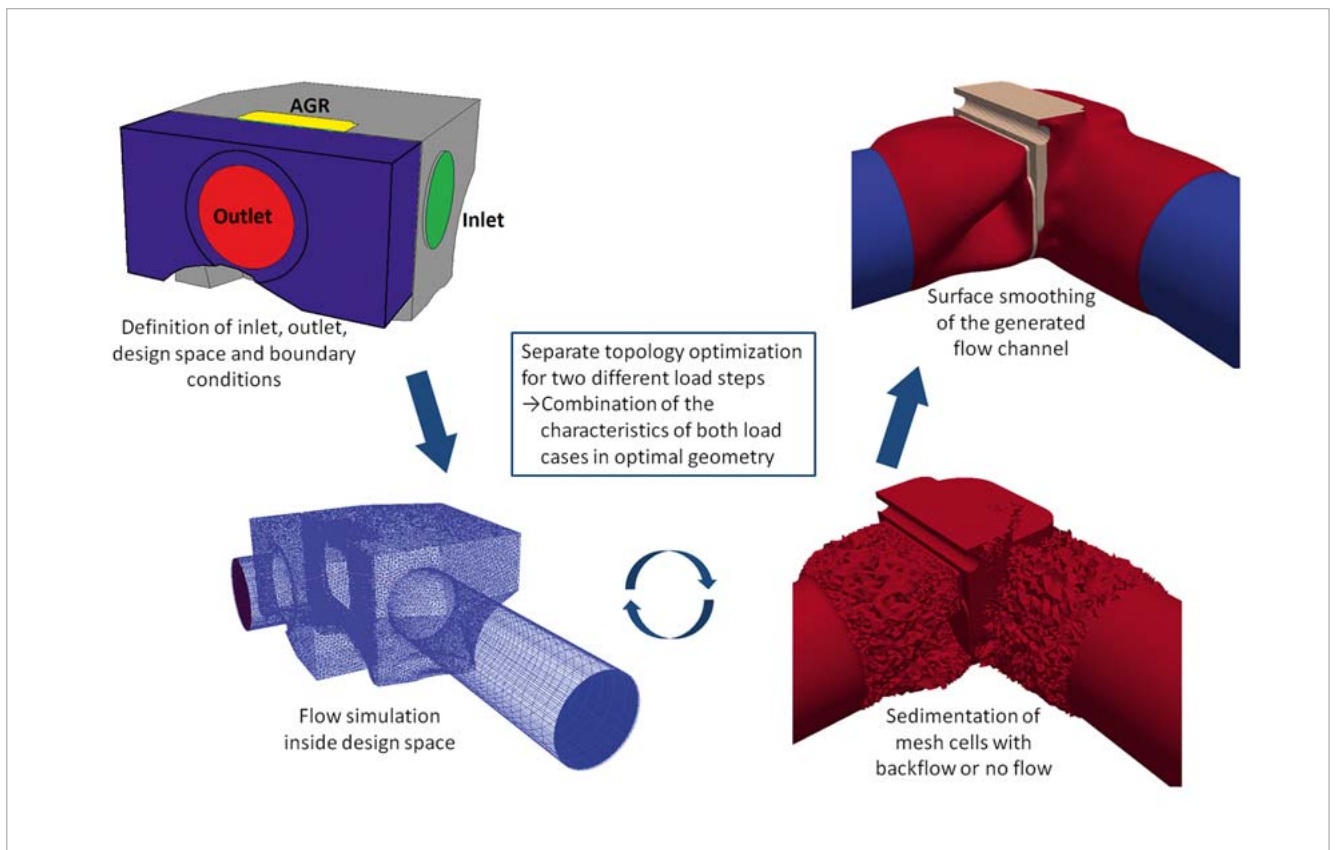


Fig. 3: Principle of topology optimization



load cases. Finally, robustness evaluations of the optimized design are executed with regard to scattering measures in the manufacturing process or in the operating conditions.

### Topology optimization

Topology optimization is a non-parametric approach (Fig. 3). In this study, the software Simulia Tosca FLUID simulates the sand deposit behavior of rivers to detect an optimal flow channel design for the available design space. Thus, it is a bionic approach which is able to result in very innovative design concepts. This is furthermore promising in the context of application of modern manufacturing processes (i.e. ALM).

This approach is typically used in tasks dealing with pressure loss reduction, flow homogenization and mass flow balancing. Since only an available design space and load case is required for this optimization type, it can be used perfectly for frontloading activities.

### Boundary conditions & design space

First, the boundary conditions for the fluid mechanical simulation are defined corresponding to the load case of interest. In the following step, locations of the fluid inlet and outlet as well as the boundaries of the design space are determined. The flap operation area is defined as non-design space. Thus, it is not possible to apply a topology optimization algorithm for the sedimentation.

### Meshing & simulation setup

The CAD design space is defined with Dassault CATIA V5 and meshed with ANSYS ICEM CFD. Afterwards, the resulting mesh is imported into ANSYS Fluent in order to define the CFD simulation model setup used by Simulia Tosca Fluid. Performing a test is recommended in order to check whether the simulation setup is suitable for a topology optimization run. The topology optimization is carried out separately for each of the two load cases with corresponding boundary conditions:

- LC1: full load, flap closed
- LC2: partial load, flap opened

### Optimization & sedimentation

During the optimization run with Simulia TOSCA Fluid, a connected ANSYS Fluent simulation is performed in the background. Additional variables represent the sedimentation behavior. TOSCA Fluid iteratively evaluates those variables for each mesh cell in the design space of the current iteration. It deactivates or sediments cells with regard to occurring backflow or no flow. Hence accessible design space is iteratively modified for Simulia TOSCA Fluid. Finally, the topology optimization algorithm converges to a flow channel contour which provides “positive” flow for all mesh elements. All sedimented elements are eliminated in the resulting geometry file.

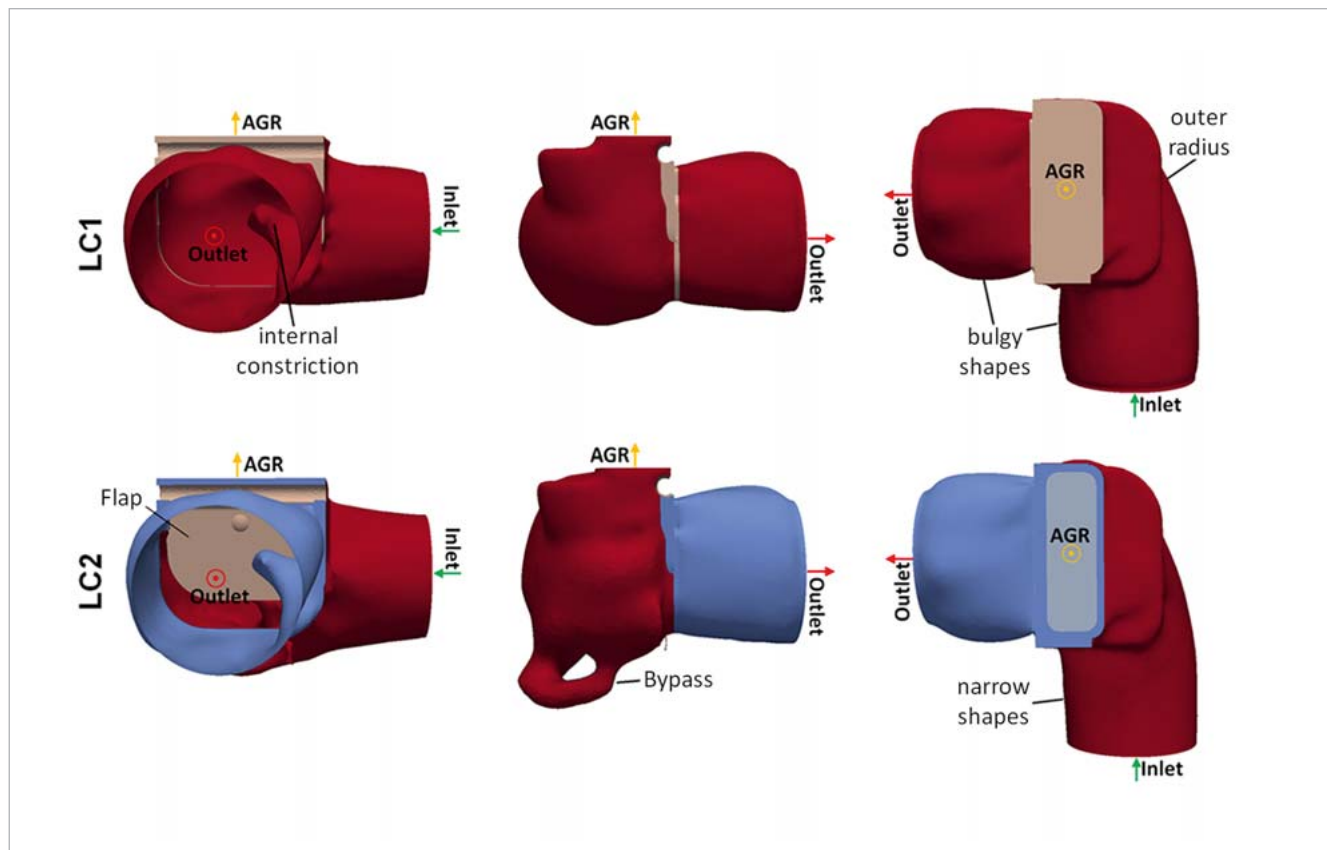


Fig. 4: Results of the topology optimization

### Smoothing & significant features

The final step in topology optimization is the smoothing process. Since the result of the raw topology optimization shows tessellated surfaces representing the unsedimented cells of the design space (i.e. flow channel contour), it cannot be used for the further CFD process. A simulation run validating the results of the topology optimization is required due to assumptions related to optimization principles (i.e. resolution of near wall flow is insufficient during topology optimization). Thus, the unsedimented mesh elements are smoothed with regard to the flow direction in order to provide a homogeneous flow channel contour. Depending on the optimization task, smoothing results may be not satisfying. Consequently, a geometry return after the topology optimization has to be performed with the CAD software. From the smoothed results of the topology optimization of the EGR flap valve, significant characteristics can be derived for both load cases.

As shown in Fig.4, increasing cross-sectional areas downstream of the inlet and upstream of the outlet resulting in bulgy shapes are noticeable. In addition, there is a continuous curvature targeting towards the outlet without considering the maximum dimension of the flap operating area. In contrast to LC1, a continuous curvature is modified in LC2 in order to provide a perpendicular flow towards the EGR cooler outlet. The bypass channel supports this effect by conducting the flow parallel to the flap position towards the EGR cooler outlet. The inner constriction (blue face in Fig. 4) is a significant characteristic at the outlet but cannot be manufactured because of demolding restrictions.

### CAD-implementation

At first, only the flow channel is modeled and parameterized by the design department. Afterwards, the flap with its associated connection to the EGR cooler as well as the draft angles are added to the CAD model. Spline curves are used to represent the complex surface of the flow channel

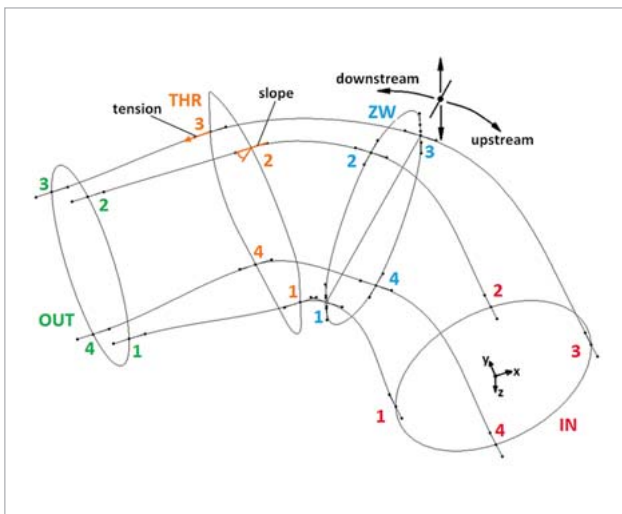


Fig. 5: Generation of a CAD-geometry

contour resulting from topology optimization runs. For this purpose, the smoothed resulting geometries from Simulia TOSCA Fluid are visualized using a line curve model, which is derived from cut planes located orthogonal to the main flow direction in specified intervals.

In order to create a parameterized CAD flow channel, which is capable of accurately representing the results from the topology optimization, a total of four supporting cross-sections are defined (Fig. 5): the inlet (IN), the outlet (OUT), the flap seat (THR) and the intermediate position between inlet and flap (ZW). The last one is variable parallel to the flow line. The four cross-sections are connected via spline curves with an offset of  $90^\circ$  (along circumference) at four support points (1, 2, 3 and 4). The curve stiffness and curve starting angle can be modified at each supporting point for each spline curve. The stiffness is a measure which determines the influence of the angle at a certain distance from the supporting point along the spline curve. Finally, the support cross-sections and spline curves are used to model a closed volume for the EGR flow channel. This procedure results in a total of 56 input parameters.

Afterwards, the geometry of the flap is added to the component including the connection to the EGR cooler (Fig. 6). Furthermore, geometric manufacturing restrictions are implemented. During the parametric optimization, both load

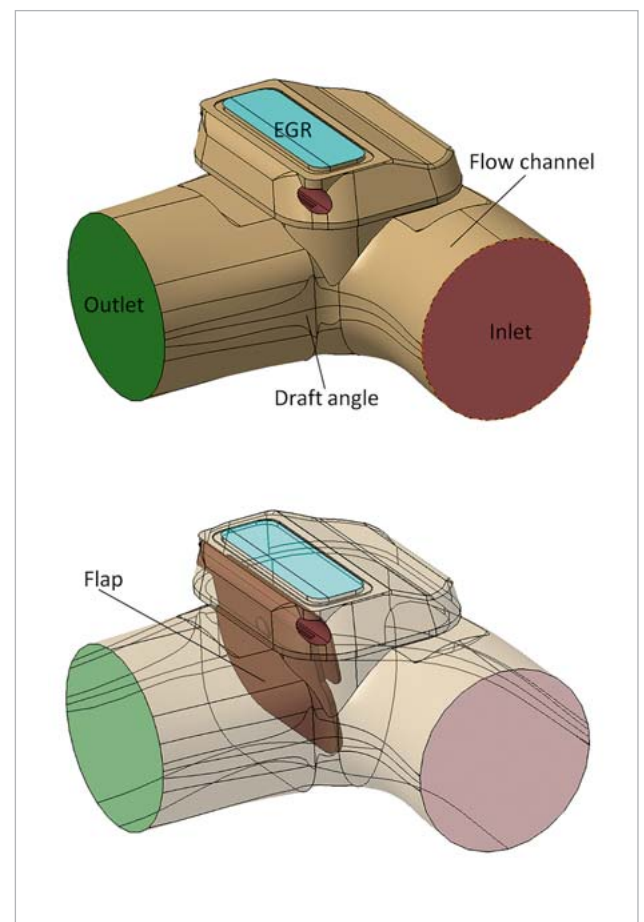


Fig. 6: Parametric CAD-Model

cases use identical flow channel contours, but the flap position differs. Thus, two models are created: one with closed flap for LC1 and one with open flap for LC2. The two resulting geometries from the topology optimization can now be represented via a certain input parameter set for each load case.

### Sensitivity analysis

A numerical Design of Experiment (DoE) is performed using state-of-the-art space-filling sampling plans like Latin Hypercube Sampling (LHS). Due to its independence from the number of input variables, a maximum of approximately 120 solver runs is required to provide a useful database for metamodeling. The input parameters (CAD, operating conditions etc.) are varied based on the DoE plan and output parameters (systems responses which are part of the objective function and constraints) are determined. The DoE results are investigated in a sensitivity analysis to identify important parameters as well as correlations and non-correlations. The resulting metamodel is a n-dimensional mathematical description of the most important correlations and interdependencies and can be used by optimization algorithms or, for example, as a pre-dimensioning tool.

### Design of Experiments (DoE) & metamodel

In this study, 148 designs (including failed designs) are generated using the method of Advanced Latin Hypercube Sampling. Due to the complexity of the geometry model, the dependencies, correlations and sensitivities of the parameters are difficult to describe. A gradual reduction of parameter limits and

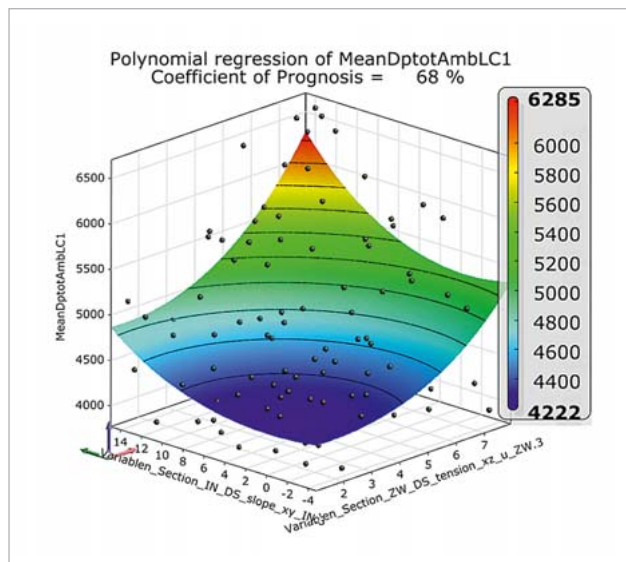


Fig. 7: Metamodel for the objective function value

the identification of superimposed parameter functions result in a re-examined 31 of the total of 56 geometry parameters of the EGR valve. This increases the prognosis quality of the response variables with regard to the input parameters. The required magnitude of 80 percent of the prognosis coefficients is thereby nearly fulfilled for the most important outputs.

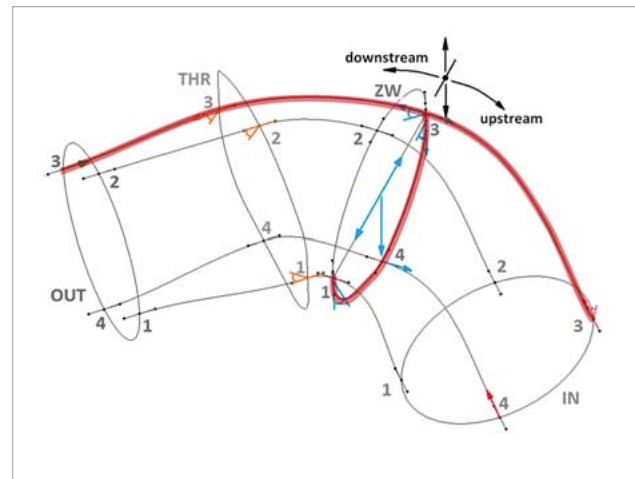


Fig. 8: Sensitive parameters on the outer surface and the lower support cross-section

The result of the sensitivity analysis is a metamodel with a total of 15 sensitive parameters with respect to the objective function and constraints (Fig. 7). The main influence is on the outer contour and the lower support cross-section of the CAD model. The arrows in Fig. 8 symbolize the tension parameters, while the angles represent the slope parameters.

### Parameter optimization

Optimization algorithms are used to vary the input parameters of the parameterized model. They minimize the objective function under the consideration of constraints. Single or multiple objective optimizations could be performed. To have a sufficient starting point for the optimization run, it is recommended to use the best design of the DoE as start design. If a metamodel with high prognosis quality is available, it is used in the pre-optimization. The Pre-optimization uses algorithms, such as Evolutionary Algorithms (EA) which are not limited to a number of input parameters but require a lot of iterations. Since a metamodel is used to determine the system response and no additional solver runs are required, more than 1000 iterations are not critical. Thus, pre-optimization is a “cheap” method which helps to identify a sensitive subspace for the final optimization. This optimization is conducted to find the global optimum in the design space. For this task, particular algorithms are used, such as adaptive response surface methods (ARSM). However, they cause limitations, i.e. max. 15 input parameters. In addition, the final optimization is “expensive” since it performs solver runs in each optimization iteration.

The objective function for optimization is defined on the basis of the output parameters which are minimized regarding the constraints. The minimization of the total pressure loss in LC1 is the most important objective valued with a rating of 60 percent. The equal distribution of the flow towards the EGR cooler is weighted at 30 percent and the static pressure loss in LC2 in the direction of the cooler at 10 percent. In order to achieve the EGR rate, it is important to develop a coun-

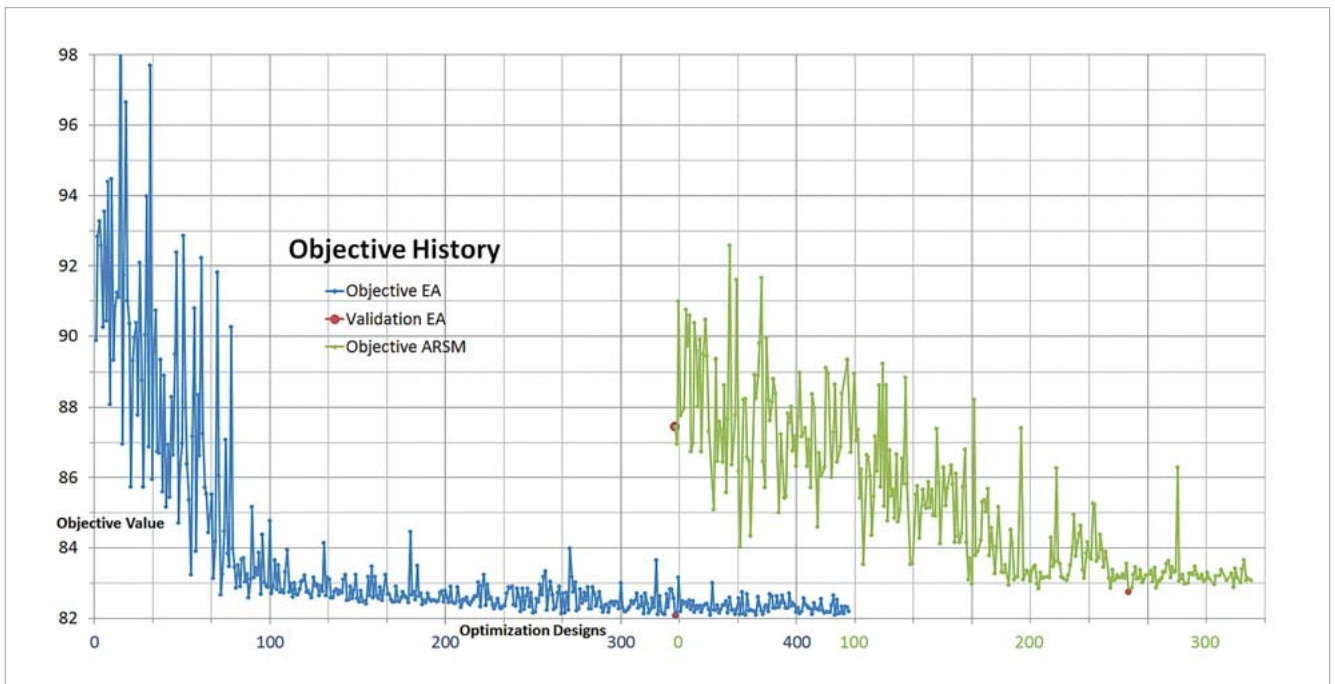


Fig. 9: Course of optimization

ter pressure in the direction of the exhaust pipe in LC2. This is defined in a constraint with a minimum value for the static pressure loss. Furthermore, the resulting forces on the flap must not be larger than in the reference model.

### Global pre-optimization

The pre-optimization on the metamodel is performed using the entire data set of the sensitivity analysis. The best designs of the sensitivity analysis, regarding the objective function and constraints, are used as a starting population for the optimization using an evolutionary algorithm. Due to the prognosis values lower than 80 percent from the sensitivity analysis, it is difficult to find an optimal design, which can be confirmed by the validation computation. After several runs of generating predictable metamodels, a design was determined indicating the lowest value in the objective function. Nevertheless, it deviates from the value of the metamodel prognosis.

### Final optimization

For the final optimization, the parameter set is reduced to the 15 most sensitive parameters derived from the sensitivity analysis. The best design of the pre-optimization is used as a start design. The result of the optimization is a further improvement compared to the validated solution of the pre-optimization. The inaccurate prognosis of the optimization on a metamodel can nearly be achieved regarding the result value (Fig. 9).

### Result of the parameter optimization

In comparison to the optimal geometry from the topology optimization, some significant similarities and differences occur in the shape of the flow channel (Fig. 10). The evolution of the

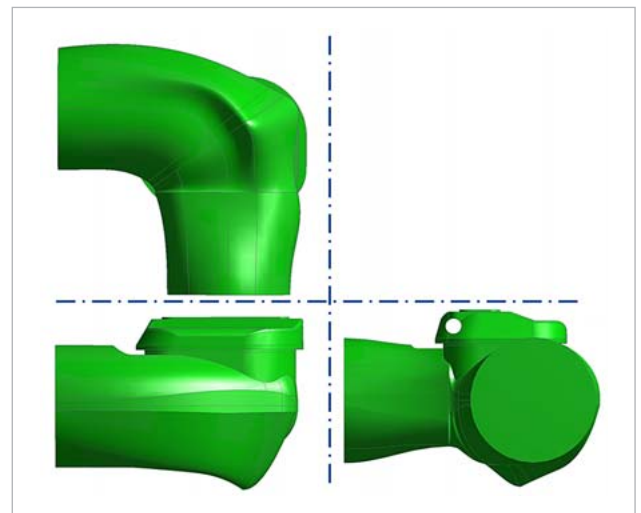


Fig. 10: Result of the parameter optimization

bypass is very noticeable in the geometry derived from the parameter optimization. However, compared to the topology optimization, the same extent of shape development cannot be observed. The inner restriction does not occur as a result of the parameter optimization. As another characteristic outcome of the topology optimization, the bulgy shape at the inlet as well as the outlet to LC1 does not appear as a result of the parameter optimization. The tendency is rather towards the narrow connection at the inlet, which is the result of the topology optimization in LC2.

### Robustness evaluation

A robust design is defined as a part which is less sensitive towards inevitable scattering of input parameters (material, geometry, load cases etc.). Thus, the variability of the



product behavior is reduced. This in return leads to an improved predictability and has a positive influence on the assessment of risk. By applying uncertainties and scattering in terms of statistical measures on the optimized design, the robustness can be evaluated (sigma level). In this study, the scattering of possible influencing factors on the flow of the exhaust gases in the valve is considered, e.g. the temperature of the exhaust gas, the mass flow, the pressure of the flow, the flap angle, the accuracy of the flap and the production tolerances of the components.

As a result of the robustness evaluation, a very dominant influence of the ambient pressure and temperature can be observed. The scattering of the production conditions causes only minimal influences. This is an important conclusion for the tolerance management in the manufacturing process. Furthermore, it can be seen that the inaccuracy of the angular adjustment has no influence on the scatter of the result values. This is also useful information for the setting of the motor operating points.

## Conclusion

Fig. 11 and 12 show the changes in geometry and its flow characteristics after each optimization step. Here, the evolution of the geometry shape can be seen. The external shape of the geometry especially changes, since the responsible sensitive parameters were determined. The locally occurring maximum pressure on the flow channel wall decreases as a result of the optimization. In addition, the pressure difference between the inlet and the outlet has dropped, which can be seen in the color scale. This is due to the changed geometry for the redirection of the flow. This feature represents a contrast compared to the topology optimization where the outer radius has a harmonically rounded shape around the flap operating area.

Fig. 11 shows the process of how the EGR valve could be optimized in comparison with the reference geometry. The continuous improvement indicates the benefit of each optimization step. In Fig. 12, the result values regarding the objective function variables are compared. The value of the objective function has decreased by 38 percent. The total pressure loss for LC1, as the most important variable, could even be reduced by almost 45 percent.

## Author //

T. Thomas, J. Jasper, T. Wanzek (Rheinmetall Automotive)

## Source //

[www.dynardo.de/en/library](http://www.dynardo.de/en/library)

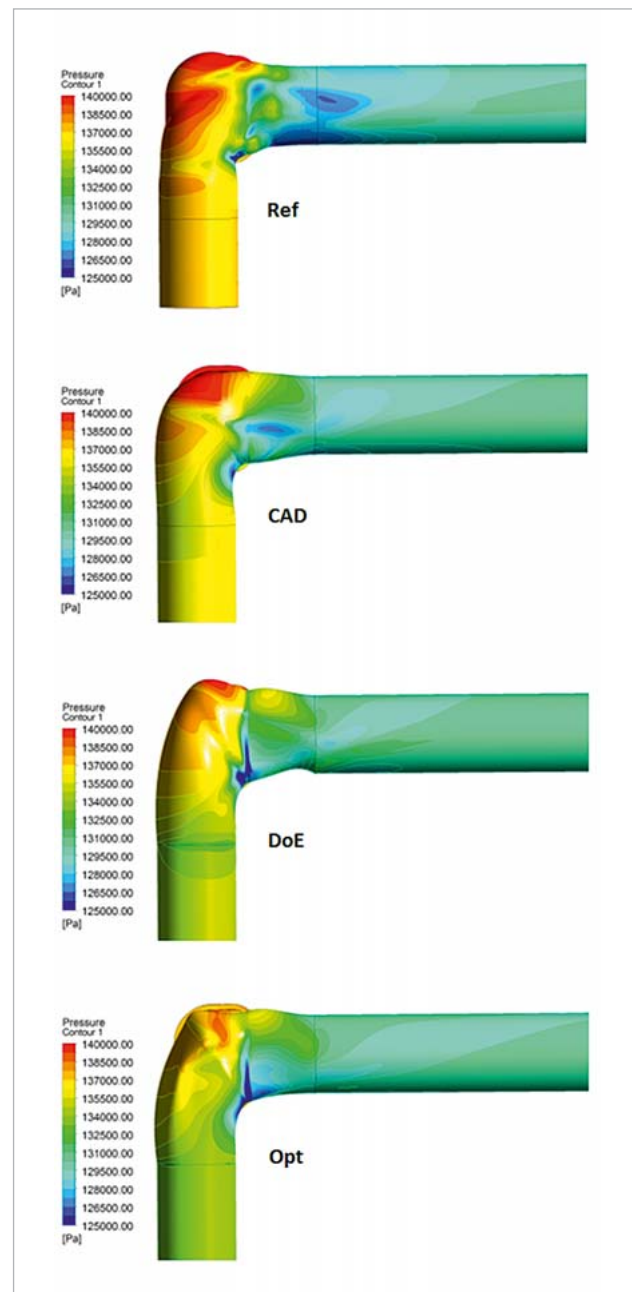


Fig. 11: Course of optimization – static distribution of pressure

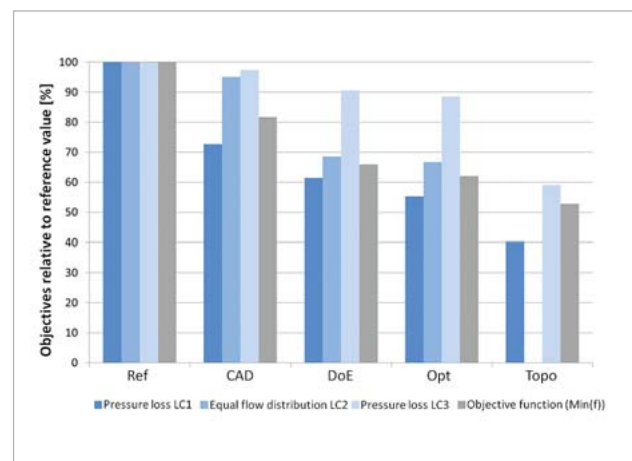
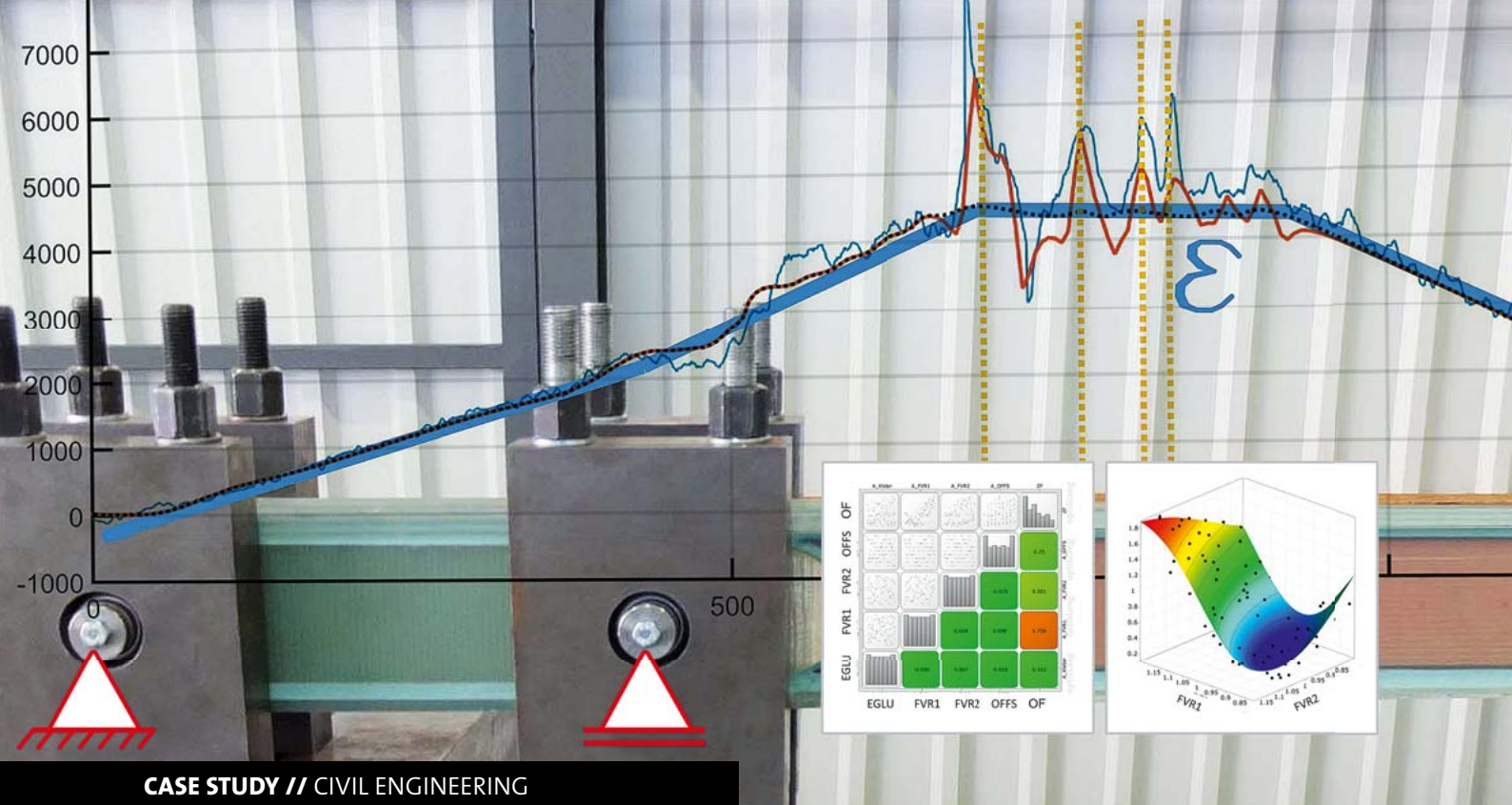


Fig. 12: Course of optimization – values of the objective function



CASE STUDY // CIVIL ENGINEERING

## PARAMETER IDENTIFICATION BASED ON QUASI-CONTINUOUS STRAIN DATA

optiSlang was applied in a strategic approach for complementing structural health monitoring by the identification of both global as well as local parameters of a structural system using data captured by high resolution fiber optic sensing.

### Introduction

What essentially distinguishes structural health monitoring (SHM) from non-destructive testing (Ndt) is the application of embedded or permanently attached sensors in combination with an automated inspection process, providing high benefit in terms of maintenance cost. Beyond that, the authors want to emphasize that a comprehensive SHM methodology should contain more than pure measurement and subsequent inspection of the acquired data, even if this task is processed automatically.

Linking advanced sensing technology to parameter identification by adequate and physically meaningful models helps to bridge the gap between mere detection of structural changes and the insight into the corresponding mechanisms. However, consequences of structural degradation (e.g. cracks in concrete members) as well as imperfections (e.g. voids in laminates) are, at least in the early stage at which SHM should take effect, spatially limited and therefore hard to detect by use of measurement principles capturing rather global structural characteristics, such as modal analysis. Though, potential locations of occurrence of the above mentioned phenomena are unknown, posing the question, where to ap-

ply locally sensitive measurement devices, e.g. strain gauges or fiber-bragg gratings. The probable existence of initial defects makes the whole task even more challenging, because in this case no reference state is available to qualify changes in structural load bearing behavior.

The objective of the present work is to complement up-to-date SHM technology by identification of both global as well as local parameters of a structural system in a strategic approach based on quasi-continuous strain data. The strain signals are gained with high-definition sensing technology using the effect of Rayleigh backscattering of light waves propagating through optical fibers. These enable to capture strain signals along the fiber's path over a length of up to 50 m with a spatial resolution down to around 1 mm. A parametric structural model is calibrated by processing the measurement data in a parameter identification procedure, in which the parameters are grouped into global and local sets. Global parameters hereby pertain to properties affecting the overall structural behavior, whereas local parameters characterize spatially limited discontinuities. The identification problem is solved using a two-step approach, in which firstly parameters of a global

reference state are determined. In a second step, the parameters of local discontinuities are identified in an iterative procedure. The approach is demonstrated on a test structure representing the load carrying component of rotor blades of wind energy plants and consisting of several GFRP-laminate parts. During assembly, these are bonded to each other by glue layers, which in industrial practice turned out to be prone to imperfections, particularly air inclusions.

### Parameter Identification

The large field of system identification can be divided into the domains of model-free black box systems and model-based gray box systems. While black box systems are represented by a set of mathematical expressions, gray box systems consist of a model containing a set of physically meaningful parameters. Their determination in a model-based system is called parameter identification or parameter update. In the field of SHM applications, this procedure enables the investigation of causes of changes in structural characteristics such as damage, initial faults or any loss of strength, rather than to merely detect their presence. Basically, the identification process is an iterative minimization of a vector of residuals  $\epsilon$ , which contains the deviations between measured output variables  $\mathbf{u}_m$  of a structure  $S$  and corresponding computed outputs  $\mathbf{u}_r$  (Equation 1) of a model  $\mathbf{SM}(\mathbf{P})$  due to an input  $\mathbf{f}$ , where  $\mathbf{f}$  in case of mechanical systems represents the structural load and  $\mathbf{P}$  the parameter vector of the system (Fig. 1). The set  $\mathbf{P}$  of parameters  $P_i$  is determined by minimizing the objective function  $J$  with respect to the vector of deviations  $\epsilon$  according to Equation 2:

$$\epsilon(\mathbf{P}) = \mathbf{u}_m - \mathbf{u}_r(\mathbf{P}) \quad (1)$$

$$J(\mathbf{P}) = \epsilon^T \epsilon \rightarrow \text{MIN} \quad (2)$$

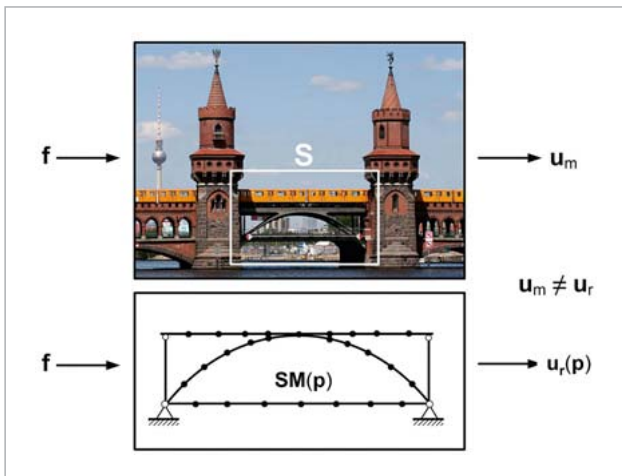


Fig. 1: Structure  $S$  and structural model  $\mathbf{SM}$  under load  $\mathbf{f}$  with responses  $\mathbf{u}_m$  and  $\mathbf{u}_r$ .

The objective function is in many cases defined by the well-known least squares regression method and its minimization represents an optimization task, which can be performed by use of a variety of different optimization methodologies.

Modal properties as natural frequencies and mode shapes are comparatively easy to gain and offer information of high density about a structures global behavior. Therefore, in the majority of applications, dynamic properties of systems are used for parameter identification. Static answers are usually more elaborate concerning instrumentation and application of test loads. Local discontinuities, such as cracks or initial defects, have only little or even hardly measurable effect on the global outputs of structural systems, independently from being of dynamic or static nature.

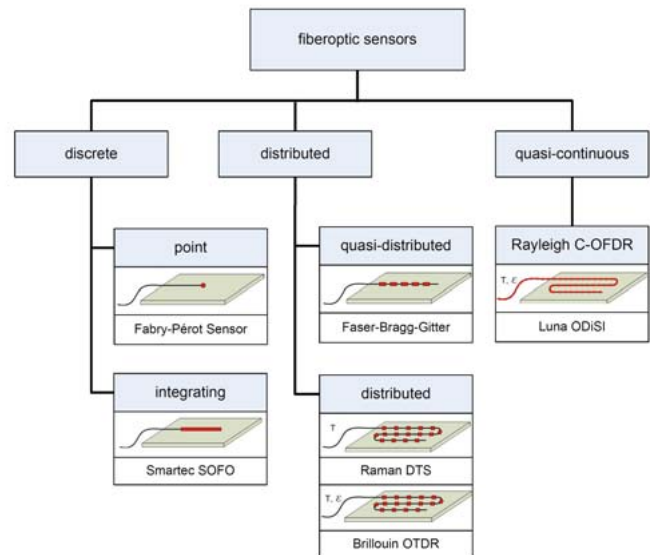


Fig. 2: Outline on sensor topologies

By understanding every structure's properties to be rather of global or local nature, it seems promising to separate parameter identification into steps, which firstly focus on global characteristics and are aimed in a second step to identify local properties such as damage.

### Rayleigh-based fibre optic sensing

Fiber optic sensors have intrinsic properties which make them ideally suited for applications in the field of SHM. Single, multiple or a great many of sensors can be realized in a single fiber of diameter around 200 microns or even less. They resist rough environmental conditions such as strong magnetic fields, chemical aggressive media as well as high temperature or radioactive radiation. Beyond that, their small scale qualifies them for installation inside and on surface of components respectively. Besides, the possibility of realizing many sensors in a single fiber helps reducing cost.

### Fibre optic sensing topologies

Fiber optic sensing systems may be categorized on the basis of their topology as diagramed in Fig. 2. In the present work, strain sensing based on Rayleigh backscattering evaluated by coherent optical frequency domain reflectometry (c-OFDR) was used. This technology allows for the definition of a very large number of sensors in the fiber, leading to

extremely high spatial resolution of the captured strain signal. In the sense of digital (discrete) data processing, the signal can be regarded as continuous, although this is not correct in a strict mathematical sense. Therefore the designation quasi-continuous is proposed by the authors.

### Rayleigh OFDR strain measurement

Sensors in a c-OFDR system can be realized in commercially available telecom fibers without any special adaption such as writing bragg gratings. The measurement principle is based on the analysis of the backscattered portion of light sent into a fiber, which occurs due to inevitable disturbances. These appear in every material and so they do as well in optical fibers. Quantity, length and position of sensors are determined in the measurement unit, dividing the length of the sensing fiber into a number of equally spaced segments (Fig. 3, top), each of which being one sensor. A light pulse sent into the fiber by a tuneable laser source is superimposed with a reference signal in a Mach-Zehnder interferometer and the interference of measurement and reference signal is evaluated in the measurement unit for each of the segments. It is beyond the scope of this contribution to go into further detail and a more elaborate description of the principle by Samiec is publicly available. Accuracy and Sensitivity as well as noise level are comparable to strain gauges or fiber bragg gratings, although the dynamically usable frequency range is (to date) rather limited.

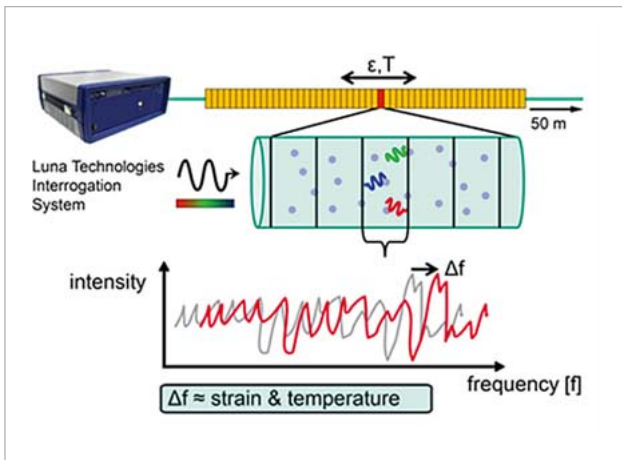


Fig. 3: Analysis of Rayleigh scattering (source: Luna Innovations Inc.)

### Application

Although having arrived quite recently on the market, the technology is already applied in many industrial and scientific applications. Fibers can be integrated into structural components as well as mounted on its surface, e.g. by bonding.

### Parameter identification on quasi-continuous strain data

In the present work, a method for parameter identification is proposed, which, due to a two step approach, is able to determine global parameters belonging to a reference state as

well as local parameters of discontinuities, e.g. initial defects. Obviously, in the case of initial defects no intact state is measurable but fortunately, quasi-continuous strain data offers enough information to recover a state without influence of local defects which can be regarded as a reference.

### Stepwise Approach

The shape function can be formulated by a finite element model, in which, at certain locations inside the structure, a number of  $i$  discontinuities in the form of e.g. air inclusions is present, see Fig. 4. A discontinuity is characterized by the parameters of location  $fx_i$ , depth under surface  $fy_i$  and length  $dx_i$ , but basically any other cluster of parameters describing any type of discontinuity is possible. The parameters are grouped to sets  $P_i$  as stated in Equation 3.

$$P_i = \begin{pmatrix} fx_i \\ fy_i \\ dx_i \end{pmatrix} \quad (3)$$

The scalar shape function, i.e. the strain signal, can be written according to Equation 4, taking into account that the relationship inside the function is represented by the finite element model. The model should allow for covering a number of  $i$  discontinuities, so that the final shape function  $N$  is a linear combination of  $N1, N2 \dots Nn$ .

$$N_i = N_i(P_i) = N_i(fx_i, fy_i, dx_i) \quad (4)$$

Loading the structure consequently yields to the formation of a peak in the strain signal whose shape is linked with the parameters of location and extent of the discontinuity. Therefore the local signal shape is defined indirectly, based on parameters of the finite element model. This, in turn, implies that the character of the discontinuity has to be known to a certain degree, which also provides for physical meaningful results.

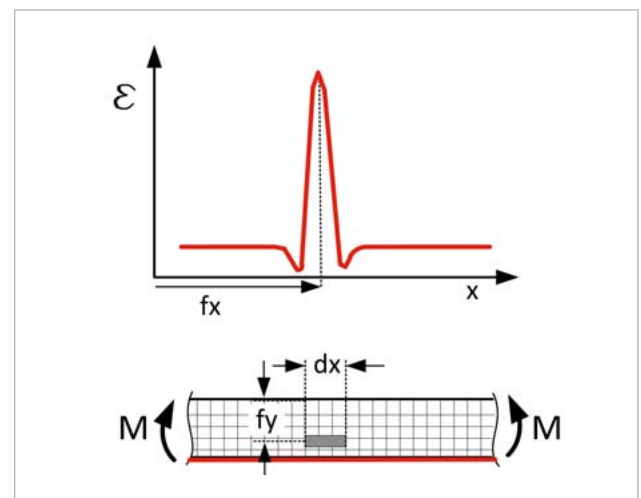


Fig. 4: Shape function used in the stepwise approach; upper figure: shape function, lower figure: structure; sensor path highlighted in red; load represented by bending moment



### Procedure

The identification process is divided into a global step and a local step, in the following called step A and step B respectively, see Fig. 5. The result of step A, i.e. set A, containing the identified global parameters, is passed to step B and is fixed

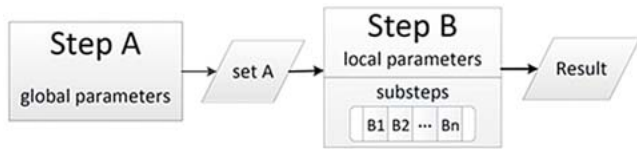


Fig. 5: Simplified scheme of the stepwise approach

in the subsequent identification of the local parameters. The method should not be limited with respect to the number of discontinuities and therefore step B runs iteratively with substeps B1, B2, ..., Bn until reaching an exit condition. At the end of step B, global and local parameters are identified. In both steps the sum of least squares of all support points (i.e. strain values of all sensors) is used as objective function.

Roughly speaking, the computational effort of solving an optimization problem depends exponentially on the number of parameters. Grouping parameters into physically consistent sets in the way shown above is therefore not only advantageous in terms of meaningfulness of the solution but also with respect to efficiency. In the method presented here, the parameter space is divided into independent subspaces allowing for the solution of several small optimization problems instead of one large task.

### Simulation example

The process should be demonstrated in this section by use of a simulation example. It consists of a simply supported beam which is loaded at two points by equal forces, as shown in Fig. 6. Global parameters of the system are the distance  $len1$  be-

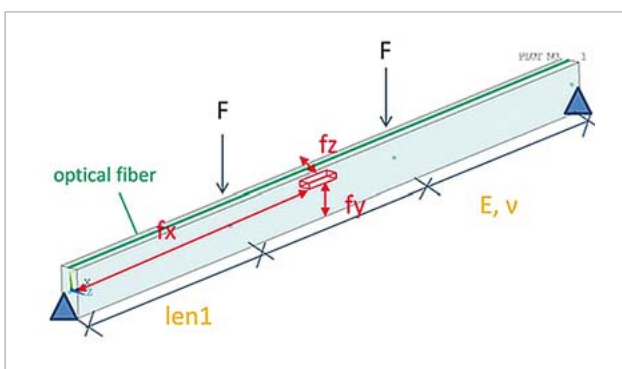


Fig. 6: Simulation example simple beam in 4-point bending test; yellow - global parameters, red - local parameters

tween one of the load points and the adjacent support, the Young's modulus  $E$  and the Poisson's ratio  $\nu$  of the material. Local parameters are the location index  $nx_i$  in longitudinal direc-

tion, the location  $fy_i$  in the cross-section in direction of the load and  $fz_i$  in the cross-section in direction perpendicular to the load direction. This test setup generates in the (virtual) sensor a strain state as depicted as reference in Fig. 7.

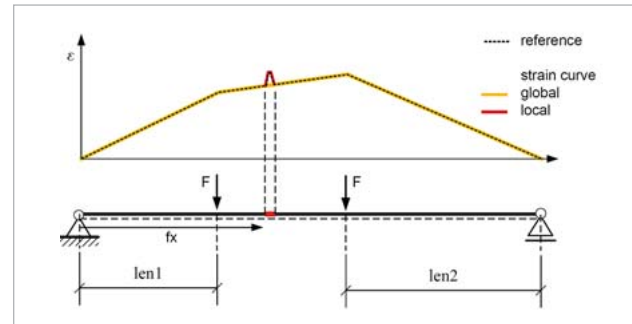


Fig. 7: Strain curves due to global and local parameters

It can be divided due to its causes into a signal of global and local strain respectively. Evaluating the objective function in a sensitivity analysis and subsequently generating a response surface, the fundamental difference in character of global and local signals is clearly visible. The response surface for step A is showing a smooth, monotonic and convex shape with a well defined minimum as can be seen in Fig. 8a while it shows a single, sharply bounded minimum in within an area of low gradient (Fig. 8b).

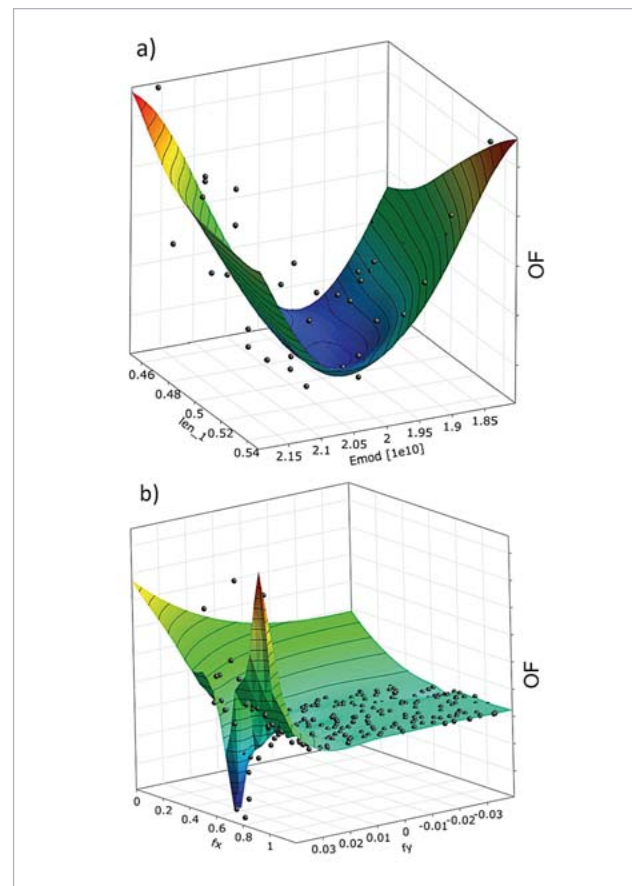


Fig. 8: Response surfaces for step A parameters and step B parameters

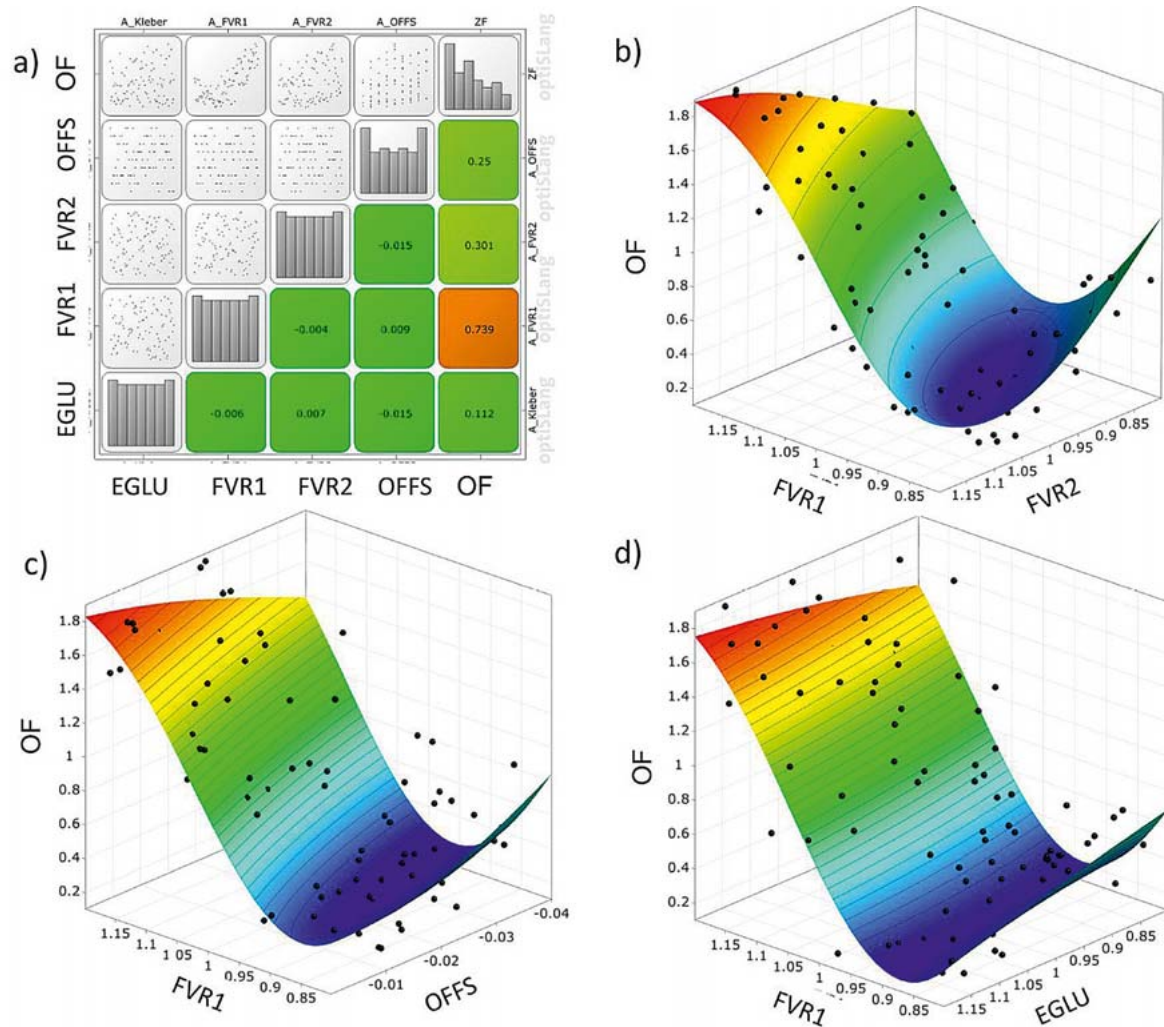


Fig. 9: Extended correlation matrix (a) and meta models (b -c) for 1-step approach

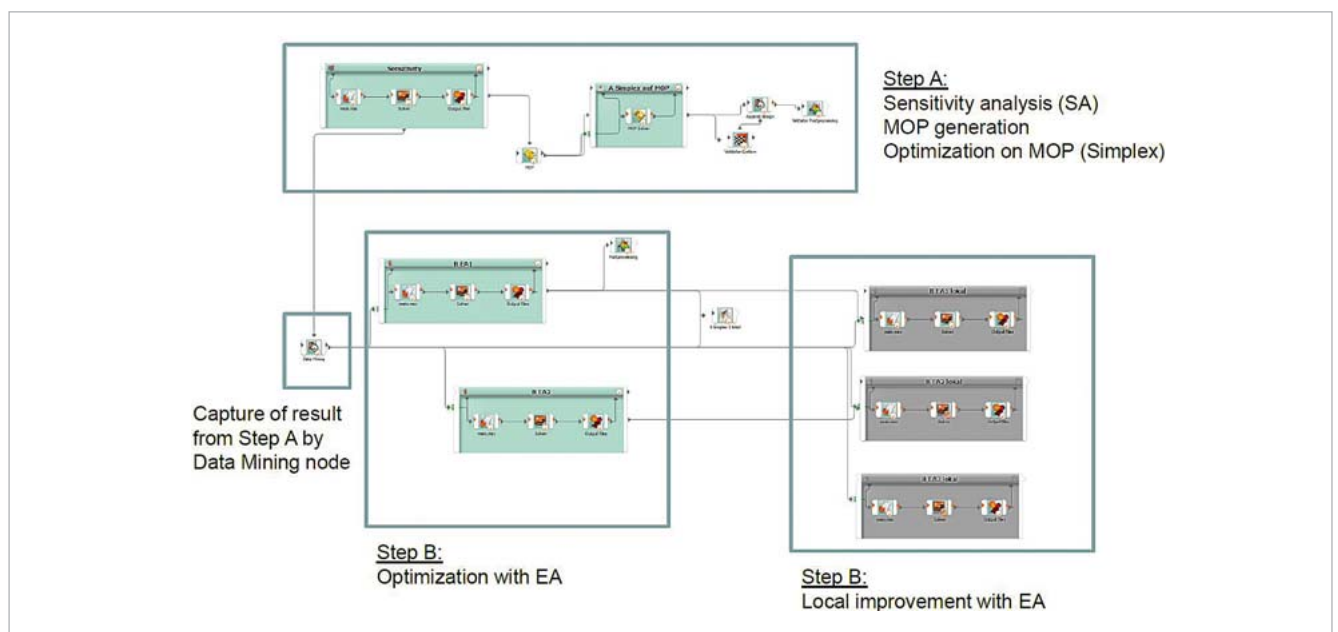


Fig. 10: Implementation of the 2-step approach in optiSlang

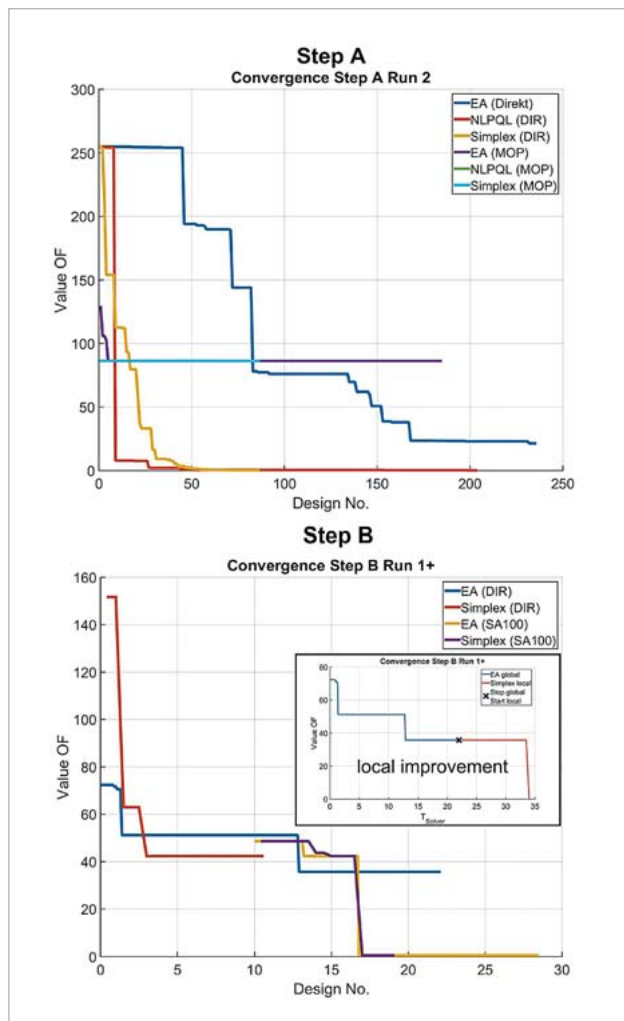


Fig. 11: Performance comparison of optimization algorithms in step A and step B

This determines the kind of optimization algorithm to be used for the minimization of the objective function. For step A, basically any algorithm is able to deliver a sufficient solution, although gradient based or simplex optimizers show better performance. For step B, random sampling based optimizers such as evolutionary algorithms are preferable. In this work, performance aspects were elaborately investigated. However, their discussion goes beyond the scope of this article.

All parameters, global as well as local, were identified properly by the application of the method proposed here whereas a one-step approach can only deliver the global parameters. This can be explained by the low impact of the local peaks in the strain signal on the objective function. The extended correlation matrix Fig. 9a shows this relation: Only the global parameters LEN1 and EMOD have significant influence on the objective function (ZF) whereas correlation coefficients of local parameters (nx, fy) are almost zero.

The setup in optiSlang shows Fig. 10. Step A starts with a sensitivity analysis to assess input parameters with respect to their importance followed by the generation of the

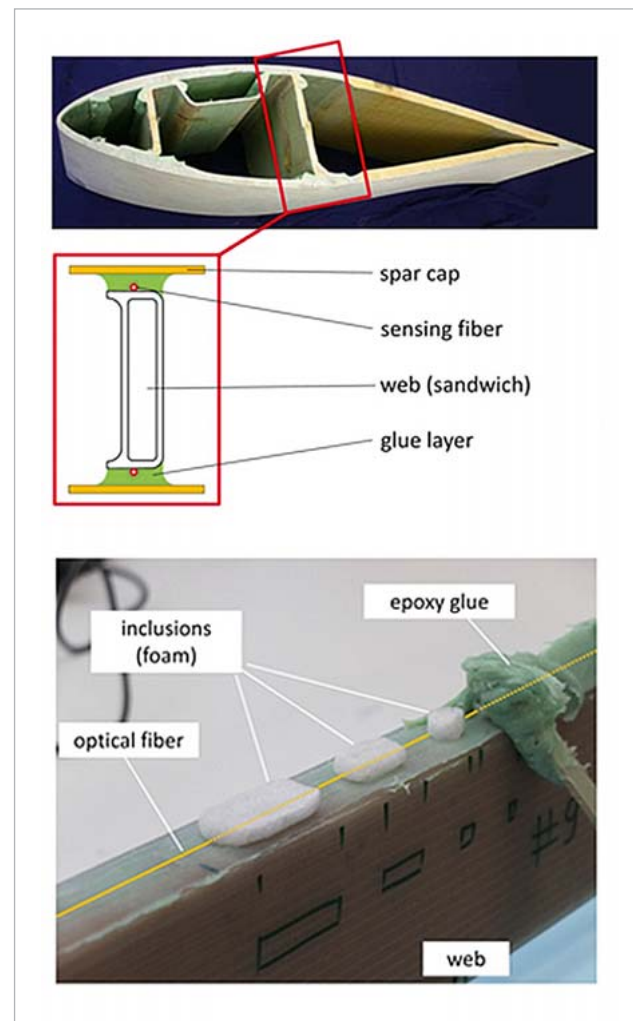


Fig. 12: Test specimen; Subcomponent of rotor blade of wind energy plants and its assembly; air inclusions are simulated using foam bodies

metamodel (MOP). The optimization is subsequently carried out on the MOP and its result is validated. Due to the rather smooth and convex character of the response surface, use of a simplex optimization algorithm delivers both accurate results and good performance. A data mining node helps to capture the optimization result and to hand it over to step B of the procedure in which local parameters are identified by an optimization with an algorithm of rather global nature such as an evolutionary algorithm (EA). The quality of the result of this step can be improved with a following iterative process. Aspects of the selection of appropriate optimization algorithms were already discussed above and can be affirmed by comparison of the performance of different algorithm types in this simulation example Fig. 11.

### Experimental application

The stepwise method described above was applied to the test of a subcomponent of rotor blades of wind energy plants shown in Fig. 12. Development and use of this component is described in detail by Sayer et al.. It consists of GFRP-laminated spar caps and a sandwich web structure bonded to

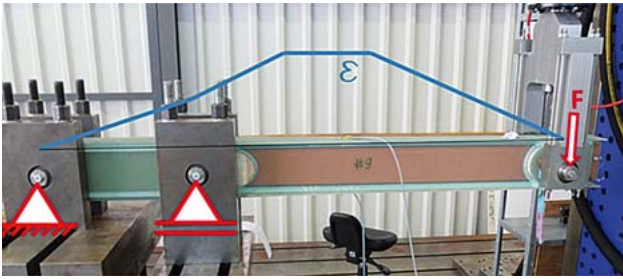


Fig. 13: Test setup for rotor blade component; shape of strain signal in blue

each other by epoxy-based glue. The objective of the investigation shown here was to detect representative voids inside the glue layer which appear during manufacture. For this purpose, optical fibers were integrated into the bondline by mounting the fiber to the surface of the web as shown in Fig. 12. The component is supported and loaded as can be seen in Fig. 13 (see next page). Due to variation of the number of layers of the spar caps, a partly constant strain signal is generated which allows for the investigation of the effect of disturbances in the bondline. Global parameters to be identified were the stiffness of the unidirectional and biaxial layers of the composite components, the Young's modulus of the glue material and a variation in thickness of the spar caps. The location of inclusions in longitudinal direction as well as their location in the cross-section of the glue layer on the tension side were defined as local parameters.

In a total of 10 iterations in step B, all larger artificial voids could be identified in location and extent. As can be seen, some deviations of the simulated signal to the measured

strain signal remain. Reason is, that not all details of the rather complex inner structure could be integrated into the finite element model. However, also the identified global stiffness parameters are showing reasonable values. As effect of a number of smaller (unintended) discontinuities also visible in CT-scans (but not documented here) a lot of smaller peaks in the strain signal can be recognized.

## Conclusions

A stepwise static parameter identification method based on high-resolution quasi-continuous fiber optic strain sensing is used to identify global and local structural parameters. The approach allows for the determination of an intact reference state and local discontinuities as well. Being based on a proper structural model, these can not only be detected but also quantified. Grouping parameters belonging together in a physical sense into sets supports efficient optimization of the objective function and leads to physically meaningful results. The proposed method is applied to a specimen representing the loadbearing component of rotor blades of wind energy plants in a bending test. Initial defects in form of air inclusions in the bond line are identified with respect to location and extent. In near future, the method should be extended to dynamic applications, too.

**Author //** Andreas Künzel (Technische Universität Berlin / SDC Statik und Dynamik)

**Source //** [www.dynardo.de/en/library](http://www.dynardo.de/en/library)

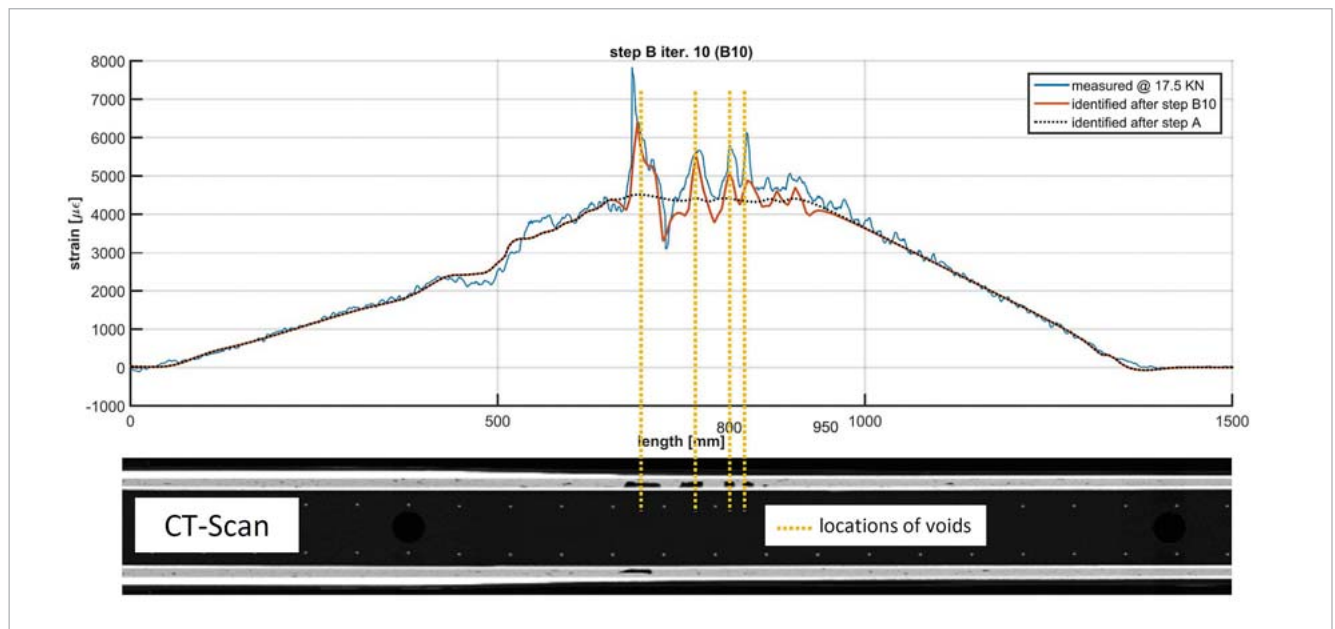
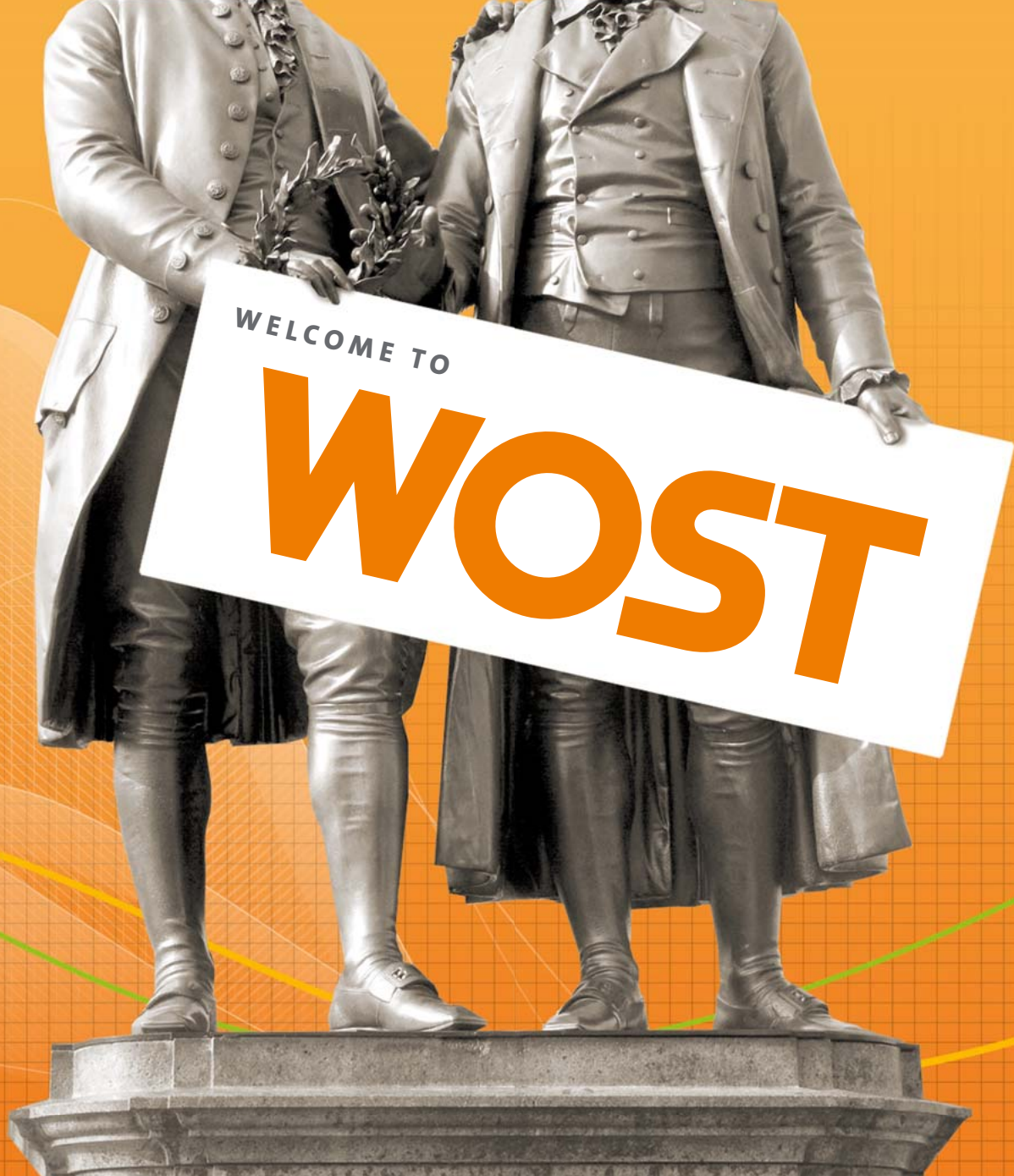


Fig. 14: Results of identification; comparison to CT-scan data





## ANNUAL WEIMAR OPTIMIZATION AND STOCHASTIC DAYS

**Your conference for CAE-based parametric optimization, stochastic analysis and Robust Design Optimization in virtual product development.**

The annual conference aims at promoting successful applications of parametric optimization and CAE-based stochastic analysis in virtual product design. The conference offers focused information and training in practical seminars and interdisciplinary lectures. Users can talk about their experiences in parametric optimization, service providers present their new developments and scientific research institutions inform about state-of-the-art RDO methodology.

Take the opportunity to obtain and exchange knowledge with recognized experts from science and industry.

You will find more information and current dates at:  
**[www.dynardo.de/en/wosd](http://www.dynardo.de/en/wosd).**

We are looking forward to welcoming you to the next Weimar Optimization and Stochastic Days.



CUSTOMER STORY // AUTOMOTIVE INDUSTRY

## ROBUST OPTIMIZATION OF CONTINUOUSLY REINFORCED COMPOSITES IN THE MOTORCYCLE INDUSTRY

At KTM, Statistics on Structures is used for the consideration of scattering production and material parameters to optimize the design phase of light-weight components used in the automotive and motorcycle industry.

### Motivation

Due to their great weight-specific properties, fiber composite materials have been currently applied in a wide range of industries. Due to high costs, in the past, they were almost exclusively used in the aerospace industry. Now, various parts in the automotive and motorcycle industry are made of this material. By combining different fiber and matrix materials as well as by the creation of laminar structures with different layer orientations, it is possible to specifically influence the mechanical properties in order to produce very light-weight components.

Although there are a variety of different manufacturing processes, all these methods have a common aspect, which is that the final material properties are set up during production, whereby the process parameters have a decisive influence on this. Depending on the type of process, scattering might occur in the production procedure. In addition to geometry and angular errors of the individual layers, these include manufacturing errors such as waviness of the fiber bundles, fiber or resin accumulations, insufficient fiber impregnation or incomplete hardening. Depending on the quality of the manufacturing process, these features can be

reduced, but not completely avoided. For this reason, it is important to know that the scattering should be taken into account in an appropriate manner during the design phase.

Based on an exemplary fiber composite structure from the motorcycle sector, a new approach using the software Statistics on Structure will be presented in this article to quantify these production scatterings and to directly transfer them back into the simulation. This opens up the possibility to consider scatterings locally in the simulation, which results in an advantage of light-weight quality compared to the application of global safety and reduction factors.

### Case study: front structure Rallye 450

The production of geometrically complex and intensely three-dimensional structures is demanding because of the limited draping capability of fiber semi-finished products. They potentially show increased production characteristics as already described. For this reason, the roadbook base carrier (RB-BC) shown in Fig. 1 was chosen as an application example for the evaluation of the developed scattering ap-



proach. In addition to carbon fibers, this base carrier also contains aramid fibers. Here, semi-finished products with woven fabrics of the type “twill 2/2” are applied.

The main function of this base carrier is the load-carrying of the IriTrack, a GPS emergency transmitter, as well as the connection of the light unit and the roadbook to the motorcycle frame structure. The roadbook is the paper-based navigation aid which contains all necessary direction and distance information. In addition, the panel (not shown in Fig. 1) is partly connected here.

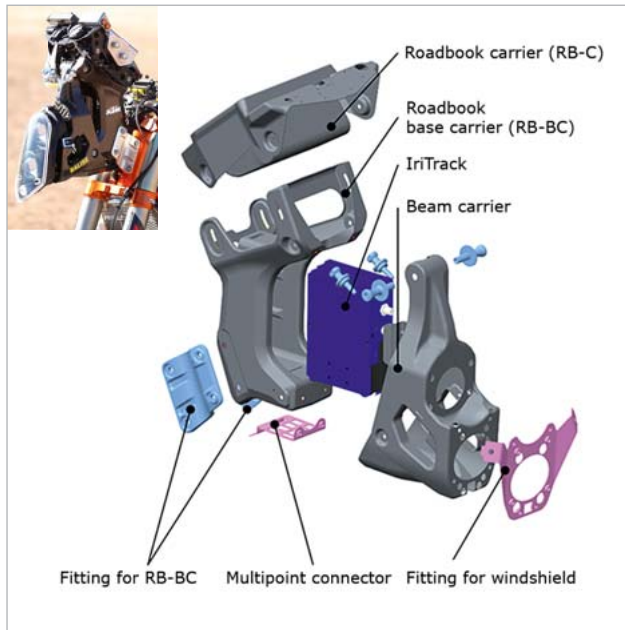


Fig. 1: Front structure of the KTM Rally 450 motorcycle: assembly view with all functional components and fittings (left) and exploded drawing of the main structural components on the right

## Overview

In order to provide an overview of the procedure, all steps are initially sketched in an application example. As a starting point, the RB-BC is used with a predefined layer structure and relevant load cases are defined. They were also selected in such a way that they could be applied with a high measuring accuracy in the experiment. The evaluated stiffness loading conditions reflect the use of the RB-BC in practice, but represent only a part of the operating load cases used for the design. A pretest analysis using Statistics on Structures determines suitable measuring points with maximum information benefit of occurring scatterings.

The three test scenarios are again carried out on three RB-BCs that are identical but slightly scattering due to the manufacturing process. In each experiment, four measurement points determined by the pretest analysis are chosen, which are also easily accessible in the experimental design. The test procedure is repeated five times in each case in order to detect the measurement errors caused by the test

facility. Thus, a total of 240 deformation values is considered. These measurement data are evaluated, applied to the simulation as reference points and used for the definition of target functions for a subsequent calibration. For the uncertainties that must be calibrated, the following parameters are introduced for the mapping of scattering properties into the simulation model:

- Layer orientation
- Layer thickness
- Material properties
- Degradation fields for the detection of further scattering

With the calibrated simulation models, robustness evaluations can then be conducted using the same parameters and conclusions can be derived from the results to improve the product quality.

## Simulation of design load cases

The loading conditions in the component design are complex and include not only static stiffness and strength loads, but also dynamic crash loads for the consideration of specific falls and rollovers. Exemplary operating and maximum loads are shown at the top and on the bottom in Fig. 2.

Since it is too time-consuming to consider all design load cases for the evaluation of the scattering methodology, they were reduced to stiffness cases for the roadbook base carrier which



Fig. 2: Exemplary samples of load cases for component design - maximum load impact upper body on roadbook (top), operating load while jumping (bottom)

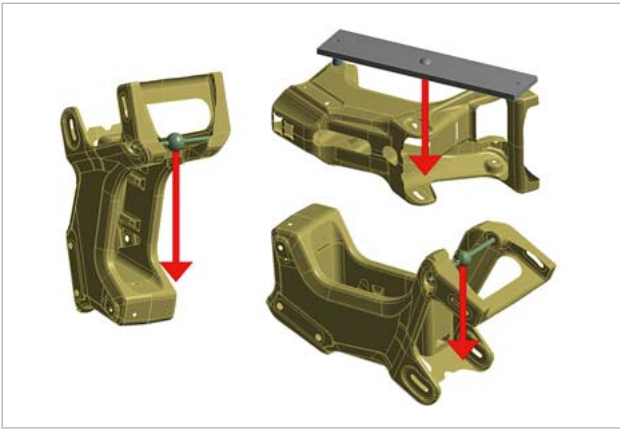


Fig. 3: Simulation setup of the three test load cases 1, 2 and 3. The areas of the support (red) as well as the point masses for the representation of the weight force are shown

is separately considered in order to eliminate the effects of the surrounding components (and their scattering) on the results.

### Simulation of test loads

Fig. 3 shows the defined simulation load cases for the RB-BC. On the one hand, these were selected in a way that they still represent the original test load scenario and, on the other hand, to ensure the experiment is conducted with as little measurement scatter as possible. They represent the essential stiffness, which can be described in the subsequent measurements by means of displacements at defined points. The modeling of the object-oriented layer structure is strictly conducted within ANSYS Composite Prepost according to manufacturing instructions, which are summarized in the so-called plybook. The orientation is regulated by the adjustment of several coordinate systems, thus allowing a fast variation of the fiber orientations.

The roadbook base carrier, which is meshed with shell elements, is joined with the load application elements via a modular building block system. Here, a consistent meshing is ensured, avoiding undesired effects from mesh noise (i.e. the influence of the mesh on the results) and spares the necessity of mapping routines for the uniform display of results in the later field statistics. The avoidance or minimization of such numerical effects is important in order to clearly separate and describe the investigated physical scatterings.

The connection of the roadbook base carrier with the fittings is represented by bonded contacts and non-linear contacts. Here again, the numerical effects have to be kept small. Thus, a study is carried out with regard to minimized tolerances in the contact regions. The weights used in the experiment are represented by mass points, which are symbolically depicted as spheres in Fig. 3. In order to calibrate the simulation model and to carry out robustness evaluations subsequently, a corresponding variability is introduced to the simulation models. For example, the modulus of elasticity, the shear model

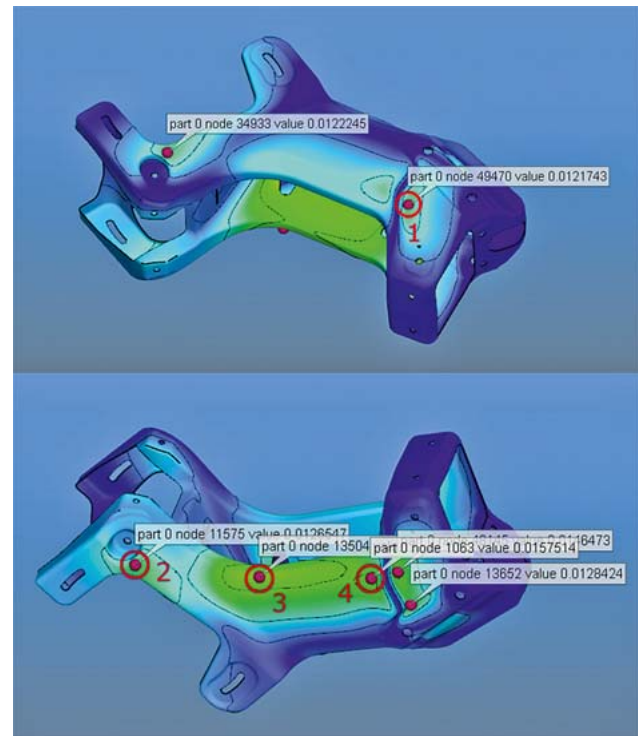


Fig. 4: Most meaningful measuring points for load case 2 determined with a pre-test analysis

as well as the layer thickness and orientation can be changed via parameter lists. Further variability is integrated by degradation fields which still will be described more detailed.

### Pretest analysis and experimental procedure

The test procedure can be summarized in three main steps:

1. Tolerance analysis in order to determine the manufacturing accuracy of the fittings
2. Pretest analysis to predict the locations for the most meaningful measurement points
3. Repeated test runs for the three load cases for detecting the deformations and the inaccuracies occurring during the measurement

A tolerance analysis is carried out first in order to avoid a situation in which the deformations measured in the test are not dominated by the deviations in the manufacturing process, but mainly by insufficiently tolerated fittings. The results are taken into account in the manufacturing of the fittings. For clamping the roadbook base carrier, a U-profile is manufactured in two parts in order to prevent tensions during the mounting of the specimen. Thus, non-parallel fitting points on the specimen can be compensated. Pretest analyses are conducted afterwards. Here, scattering is applied to the still not calibrated simulation model, variation calculations are carried out, and average values, standard deviations and variation coefficients are evaluated by superimposing the field results. The variation coefficients indicate information about the correlation between experiment and simulation.



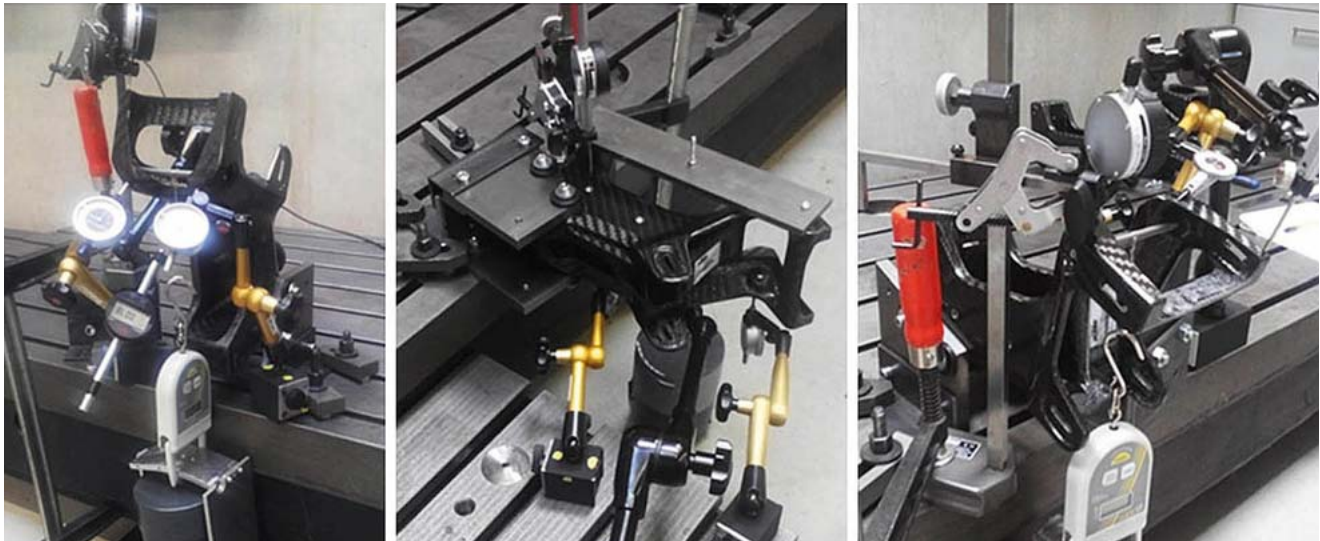


Fig. 5: Experimental setup for load cases 1, 2 and 3 carried out at the Chair of Engineering Design (KTmfk) at Friedrich-Alexander-University Erlangen-Nuremberg

Therefore, the dial gauges are not placed at the locations of the maximum deflection but at the places of the presumed greatest variation of deformations. Fig. 4 shows the result of such an analysis. Suitable measuring points are determined by a hot spot detection. The red marked spots are selected for the measurement, considering the necessity of an easy accessibility in the experiment.

Fig. 5 shows the setup of the experiments. The specimen is clamped in the required positions and loaded with a weight. Under these conditions, five measurements are carried out at four measuring points for each load case and RB-BC. Although the tests are conducted in an extremely careful manner, experimentally induced scattering cannot be avoided completely. Reasons can be found in varying zero adjustments of the dial gauges, in different preloading forces, in deviating positioning of the dial gauges as well as in other environmental influences.

### Use of field statistics to describe scattering

As already mentioned, the simulation model representing the experiments contains variables in order to investigate and to evaluate the scatterings. Also, the mentioned effects, such as manufacturing errors, fiber waviness of the bundles, fiber or resin accumulations, insufficient fiber impregnation as well as incomplete hardening can only be represented with an extremely high amount of calculation time. This makes the procedure economically inefficient. However, what they all have in common is that they cause a change of the local material properties. For this reason, degradation fields are introduced in ANSYS at this point, i.e. overlapping fields which can change the implemented material properties at any location by a definable factor. Because of such a factor can be assigned to each FE element, a conventional parameter calibration would no longer be possible due to the extremely high amount of resulting parameters. It can also be assumed that the scaling factors locally correlate. For this reason, random fields are

introduced for representing the degradation. By means of an eigenvalue decomposition, the fields can be described via basic functions (scatter shapes) and amplitudes. Thus, the large number of random variables in the whole field can be reduced to a small number of random amplitudes. The field can be re-assembled by multiplying the basic functions with the amplitudes and a subsequent summing up of these terms.

Fig. 6 shows three of a total of 100 artificially created degradation fields. The prognoses regarding the areas are based on the experience of CFRP manufacturing and CFRP experts at the OEM. By a different scaling of the scatter shapes, new fields can be created very quickly, which finally allows a calibration of the prognoses for the degradation locations with regard to the experiments.



Fig. 6: Three exemplary artificially created degradation fields

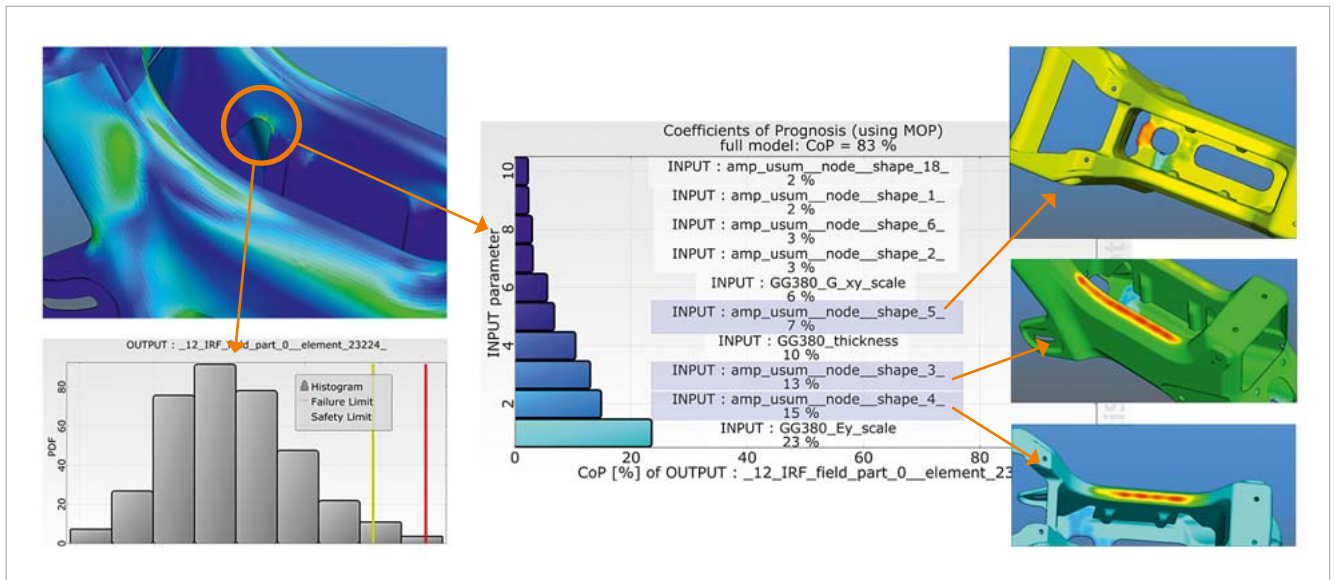


Fig. 7: Scatter influences on a specific failure point - distribution curve of the failure criterion, influence on the most important input scatterings, translation of the most important amplitudes into degradation regions (for illustrative purposes)

By using random fields for the creation of degradation fields, their descriptiveness contributes to the understanding of the functional correlation between the location of the degradation and the resulting influences on stiffness at different locations of the RB-BC. In other words, the visualization of the most influential scatter shapes helps to understand at which locations production-induced material weaknesses have a great influence on product properties.

### Calibration of the simulations to the test results

The following parameters are now available for the calibration of the simulations to the test results:

- Material properties (elasticity modulus transversely directed or in fiber direction, shear modulus)
- Layer thickness
- Layer orientations
- Amplitudes of the scatter shapes for describing the degradation fields (representing of further effects as already mentioned)

In order to calibrate the simulation results to the test results, optimizations are carried out for each roadbook base carrier. The aim is to minimize the deviation simultaneously at all twelve measuring points. The twelve terms of the target function are weighted with regard to the reference value of the respective measurements. The still very large number of parameters to be calibrated (> 50) would lead to a high amount of calculation runs. For this reason, in advance, sensitivity studies are performed in order to separate the unimportant from the important parameters and to eliminate them in the subsequent optimizations. The use of twelve measuring points in the target function increases the probability of a clear result.

### Conclusion

Now there are answers to several important questions:

- Which parameters must be set to represent the current behavior of the RB - BC?
- Which parameters influence which type of stiffness to what extent?
- How accurately can the correlation between the input parameters and the stiffness be described?

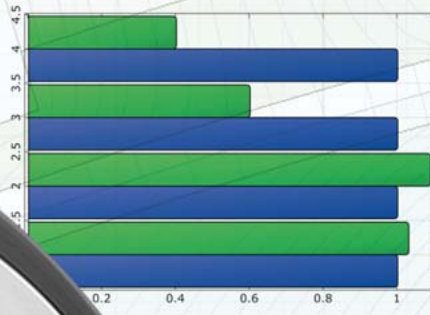
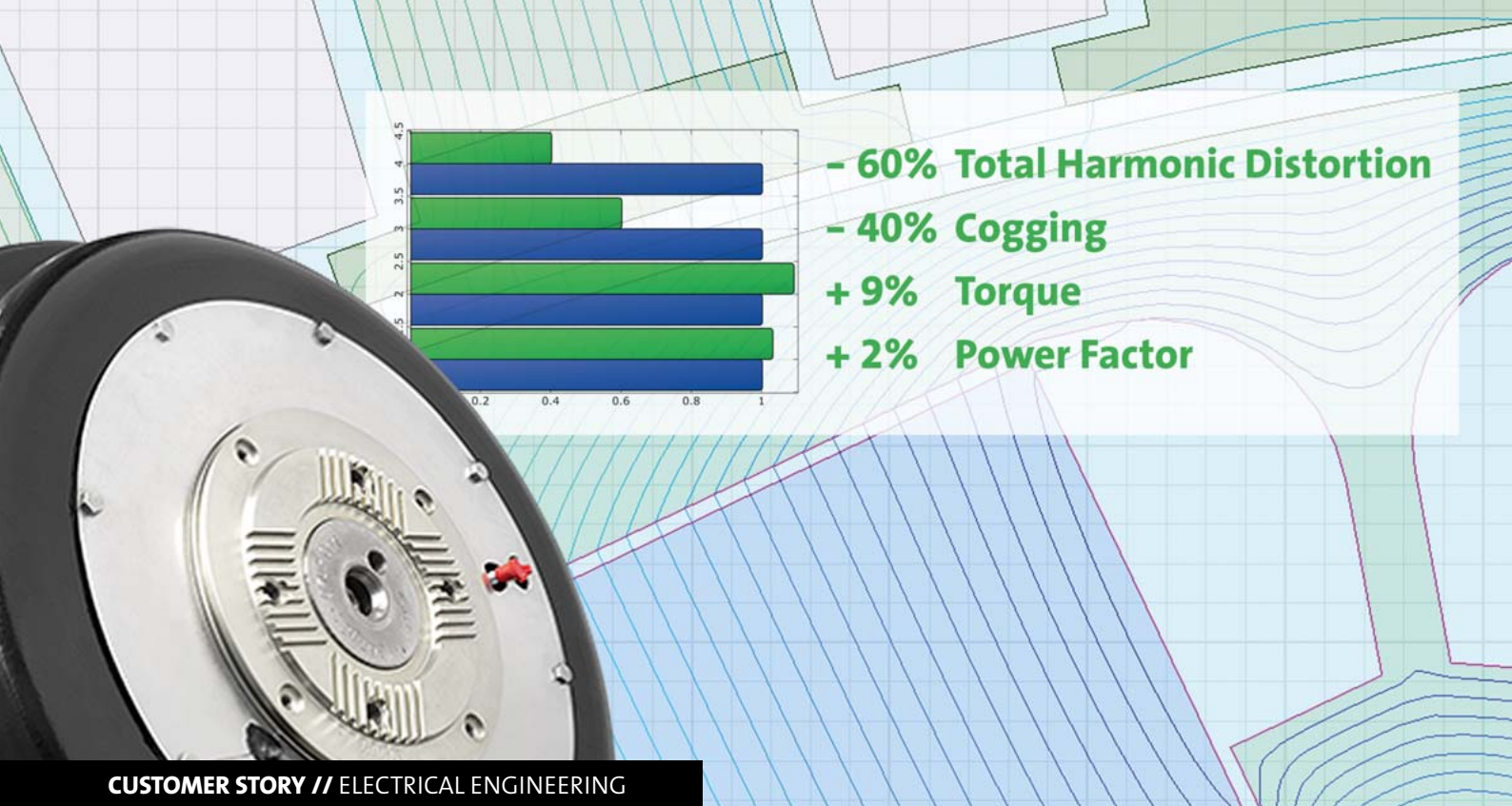
Answering these questions is necessary for a meaningful robustness evaluation and target-oriented optimization. Scattering is now applied to the calibrated scalar parameters and degradation fields. With more than 100 calculations, the scatter of the stiffness, the failure criteria and other properties can be estimated. Even more important is the capability to identify the influence of the input variables on the stated output variables.

Thus, after the robustness evaluation, targeted measures can be executed at the locations with the greatest amount of influences - either manually via reinforcements or by means of design changes as well as by optimizing the already defined parameters, for example, the orientation of the layers. Fig. 7 shows the influence of the main scattering input parameters on a critical failure spot. Such information can be noted in plybooks to be considered in future production in order to minimize the failure probability of the roadbook base carrier by means of target-oriented and locally specified improvements in production processes.

**Author //** Markus Kellermeyer (CADFEM GmbH) / Martin Perterer (KTM Technologies) / Prof. Sandro Wartzack (Friedrich-Alexander-University Erlangen-Nuremberg)

**Source //** [www.dynardo.de/en/library](http://www.dynardo.de/en/library)





- 60% Total Harmonic Distortion
- 40% Cogging
- + 9% Torque
- + 2% Power Factor

CUSTOMER STORY // ELECTRICAL ENGINEERING

## OPTIMIZATION OF A SERIES PRODUCTION ELECTRIC MACHINE IN SHORTEST TIME

SIEMENS Large Drives (Nuremberg) develops high-efficiency electric machines. In cooperation with CADFEM and Dynardo, a transferable workflow was devised for automatized motor geometry optimization.

### Electric machine design means finding the perfect geometry for multiple load cases

Electric machines handle the highest energy densities and power flows within extremely small space while converting between electric and mechanical power with efficiencies up to 90-98%. Contemporary design challenges arise from ensuring high power and efficiency ratings across a broad range of loads while at the same time keeping an eye on other machine properties, e.g. with respect to noise, vibration, and harshness (NVH). Efficient simulation-based design approaches are of particular value when going from single-load-point motors (e.g. cranes, lifts) to variable load, multi-purpose applications (machining, mobility, robotics). This case study targeted the geometry optimization of the rotor of an internal permanent magnet (IPM) machine based on a 2D FEM model in ANSYS Maxwell. The conflicting goals are to keep the rotor mechanically stable while minimizing electrical steel sheet bridges between the magnetic poles, restricting magnet material usage, and shaping the rotor design. Here, torque ripples should be minimized while maximizing the torque output. An additional goal deals with avoiding higher-order harmonics in the driving electric circuit by minimizing the so-called total harmonic

distortion (THD) of the back-EMF (electromotive force). This means facing a multi-criteria optimization problem formulated for a multi-load-case simulation. This task was efficiently solved with purely meta-model-based global and local optimization.

### The MOP and what-if questions

A thorough sensitivity study scanning a broad design space is the basis for almost any investigation with optiSLang. The sensitivity study yields a Metamodel of Optimal Prognosis (MOP) for each response. The MOP captures nonlinear dependencies, not only from single inputs but also from combined influences. An MOP of high quality allows to systematically explore many different solutions to design conflict problems in short time without the need for additional simulations.

In this case study, a large design space of the internal permanent magnet (IPM) electric machine depicted in Fig. 1 (see next page) was explored purely based on response meta-models. Fig. 2 (see next page) shows the MOP for the response exhibiting the most complex behavior, the cogging torque amplitude. The plot shows nicely that varying



Fig. 1: The IPM synchronous motor: exemplary photography with exemplary geometry and marked side pockets

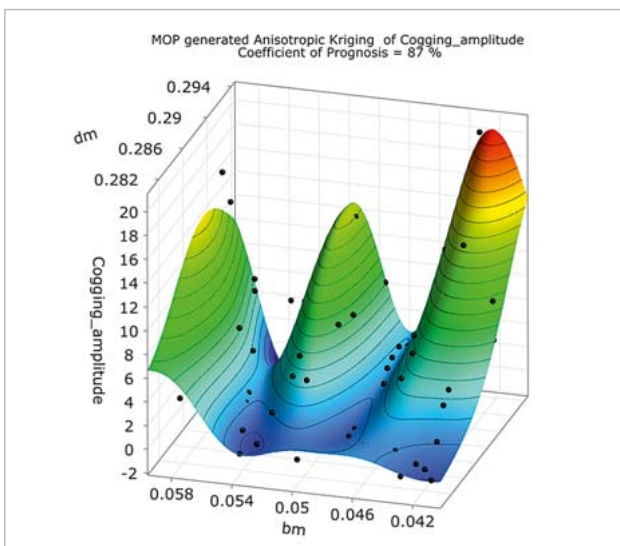


Fig. 2: MOP for the cogging torque amplitude over the two most important input variables determining the magnet size and shape. Complex responses with local minima and maxima as seen here make an optimization problem challenging, in particular when goals and constraints arising from several responses have to be negotiated.

the magnet size yields a sequence of amplitude maxima and minima. Four of the eleven varied parameters contribute substantially to the variation of the cogging torque amplitude. The plot shows only the subspace of the two most important input dimensions. By the associated Coefficient of Prognosis (CoP) of 87% an objective measure is given that the meta-model has indeed captured most of the system behavior. Only 13% of this response's variance remain unexplained by the meta-model. The other investigated responses comprise i.a. torque, torque ripple amplitude, power factor at critical load, and the THD of the back-EMF. Their MOPs exhibit even

higher CoP values based on scanning the design space with 170 successfully evaluated design variations distributed as Advanced Latin Hypercube Sampling (ALHS).

Finding an optimized design point means going to a place in the design space where the most important responses adopt desired values while other responses stay within acceptable limits (constrained optimization). Having a high-quality MOP at hand for every single response means that many interesting what-if questions can be answered. The combined set of response surfaces can answer the question as to where in the design space torque and efficiency will be maximized without compromising design constraints, such as the smoothness of the torque delivered.

“Optimization on the MOP” means that the meta-models allow the application of thorough global search strategies (e.g. evolutionary algorithms) without the need for additional FEM simulations. It also creates the freedom to experiment with different combinations of optimization goals and constraints. This is the second level of what-if questions answered: Where does the optimizer move when maximizing torque while constraining vibration amplitudes and THD? Where will the best design be found when minimizing THD while constraining the other responses? Where will Pareto-efficient designs be found in a multi-objective optimization setup?

### The optimized motor

In this case study of a high-pole IPM synchronous motor, a purely meta-model-based optimization yielded substantial improvements with respect to every single response:

- THD decreased by 60%
- Cogging amplitude decreased by 40% (see Fig.5)
- Torque at maximum phase current increased from 2540 to 2770 Nm (corresponding to a 9% increase while the magnet cross section grew by 8%)
- Power factor increased from 84 to 86%

All this could be achieved by simply varying only the rotor cross section geometry and the driving voltage phase angle. This means that tuning the stator as well will allow leveraging even further optimization potential.

## Challenges – workflow – optimized design

### Electric machine optimization challenges

Leaving the number of embedded magnets of this IPM machine constant, the rotor cross section geometry is determined by the magnet size and width, the shape of the side pockets, and the radial positioning of the magnets. Why is it not the case that more magnet material generally translates into more torque, and why is the best machine not the one with the largest magnets? Firstly, this is because



the other two materials also have a purpose. The electrical steel has the task of guiding magnetic field lines and the copper carries electric current. It translates into an economizing problem of allocating the given allowable motor volume and mass to the three materials: magnets, iron, and copper. Secondly, it is also a matter of topology: given amounts of the materials need to be distributed wisely in order to give rise to strong fields from magnets and copper windings, and to allow for these fields the strongest possible interaction. Two simple exemplary cases of misallocation can be easily understood: if the copper cross section is not sufficient, there will be excessive ohmic losses which is a drag on the efficiency and, at the same time, a cooling issue; or, as mentioned above, if the magnets are too small, their weak field means low torque.

Focusing solely on the rotor geometry, as done here, the design challenges are somewhat more subtle and involve three different aspects of the physics of permanent magnet machines: field line shortcuts, mechanical stability against centrifugal forces, and torque ripples. When magnets are embedded within the rotor's iron, this opens a flux path solely inside the rotor's steel going narrowly around the magnets sides. One speaks of flux leakage. This is why side pockets (marked white in Fig. 1) are introduced. They reduce the iron cross section of shortcut paths and force more field lines to go through the air gap and around the stator's coils. This is especially true if the machine is designed in such a way that these paths are magnetically saturated. One can see that for a given magnet size the iron topology determines whether a lower or higher fraction of the potentially available field will be used for generating output torque.

The second issue deals with the mechanical stability of the rotor. Commonly, rotors are made of sheet metal piles (reduction of eddy currents) whereby the space for positioning magnets is created by punching holes into the sheets. Thus the mechanical stability of the rotor's steel is heavily dependent on the rotor's diameter and the bridge's thickness. The design conflict becomes clear, thicker bridges mean better stability but more flux leakage.

The third issue is the one of the homogeneity of the torque over rotor position, both under load (torque ripple) and at no-load operation (cogging). It arises from the interaction of the fields of the rotor and stator and depends on the shape of the electrical steel bodies close to the airgap between rotor and stator. Similar to the torsion forces, also the local radial forces between rotor and stator are time-varying functions of the rotation angle depending on the working point. All these forces give rise to NVH side-effects.

Wrapping this up, windings and magnets create the magnetic fields and the iron guides the field lines. Motor manufacturers have to pay attention to finding an ideal cross section geometry for the rotor's steel because it crucially

influences the main design conflicts in terms of flux leakage, mechanical stability, and smoothness of operation. Variation studies with optiSLang cannot completely replace sound engineering knowledge, but they help to sort out the high-dimensional input and output parameter spaces. They help to get to better designs quicker.

### The optimization workflow

For achieving this optimization, a single sensitivity study was followed by three MOP-based optimization runs and verification simulations:

- Design of experiment (DoE): an LHS yielding a substantial fraction of geometrically infeasible designs and 170 successful simulations
- MOP results: the complex nonlinear response behavior was captured with CoP values of 87% and greater
- MOP settings: complex responses deserve meta-models made for elevated complexity like anisotropic Kriging models
- Thorough global optimization on MOPs with an evolutionary algorithm (elevated population size, 3500 MOP calls per run) in single-objective setup, i.e. one goal and several constraints, three different runs switching goals and constraints
- Gradient-based local optimization
- Two additional FEM simulations for verifying optimized designs

This case study was based on single-objective global optimizations with optiSLang's evolutionary algorithm (EA). Besides the beneficial global search properties of the EA, the key contributions to the optimization success were the definition of the goal and constraint functions and the high-quality MOPs. The EA was able to find feasible designs although constraints were formulated harsher than the responses of the reference design would have suggested which meant that none of the 170 DoE simulations fulfilled all constraints. Fig. 3 (see next page) illustrates how the EA first hits only infeasible (i.e. geometrically infeasible or constraint-violating) designs. Then feasible designs are discovered sporadically. Lastly, more and more feasible design "mutations" show up and the EA optimizes their parameter combinations or "genes" based on the principle of "survival of the fittest". That the "green insula" can be found within a "red ocean" of prohibited designs is a substantial proof of the global search capability of EAs. Other algorithms have a hard time being faced with this task under the circumstance that the system responses are highly nonlinear and not monotonic.

### The benefits for SIEMENS

This electric motor optimization workflow is beneficial for the Large Drives team, if it is more than a single lucky hit, if it is a systematically repeatable recipe for success. optiSLang sets the right infrastructure to make it repeatable with ease:

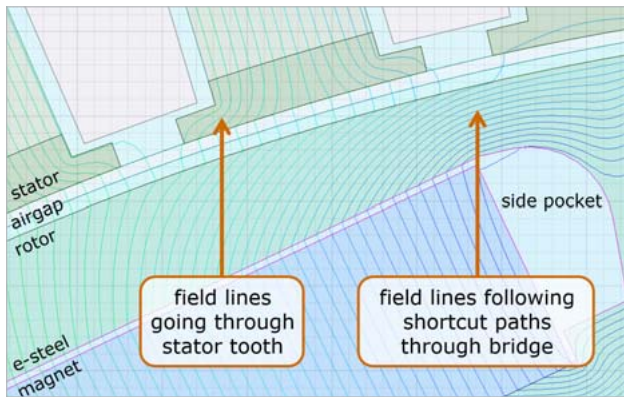


Fig. 3: Flux leakage – some field lines are not going through the stator as shortcut paths through the electrical steel bridge are available. The bridge is undesired from a magnetic point of view but necessary for mechanical stability.

- Templatization for the text-based or Workbench-based integration of Maxwell models
- Templatization for the whole optimization workflow
- optiSLang 6 allows export and import of criteria definitions
- The model parametrization does not need to be perfect, high-quality MOPs are achievable in spite of a high fraction of failed designs
- Safety infrastructure for dealing with crashes, interrupts, or database reevaluations
- MOPs answer what-if questions, (a) when the user inspects the postprocessing, and (b) when optimization algorithms explore the design space
- Instead of relying on blind runs of blackbox-optimizers, optiSLang users build on knowledge-based targeted optimization. Constantly expanding the engineering knowledge base via variation studies, data mining and causality analyses leads to long-term success

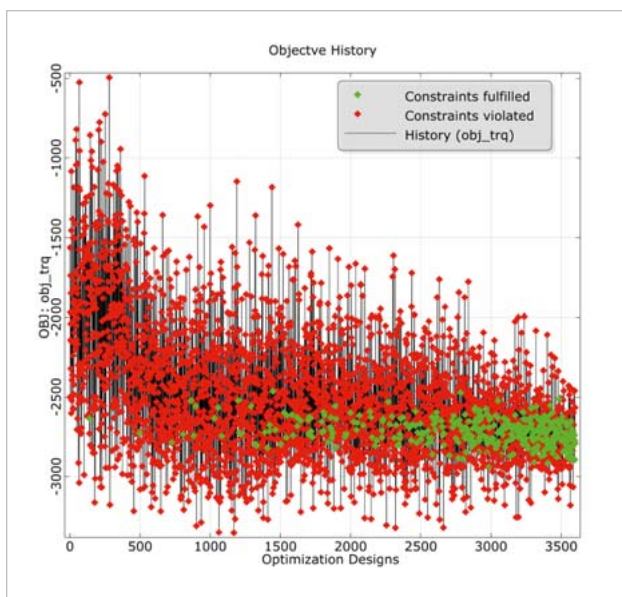


Fig. 4: EA history: geometrically feasible and constraint-fulfilling designs (green dots) first appear only sporadically. The EA principle of survival of the fittest leads to a higher and higher ratio of feasible designs and pushes the feasible subpopulation towards the optimum.

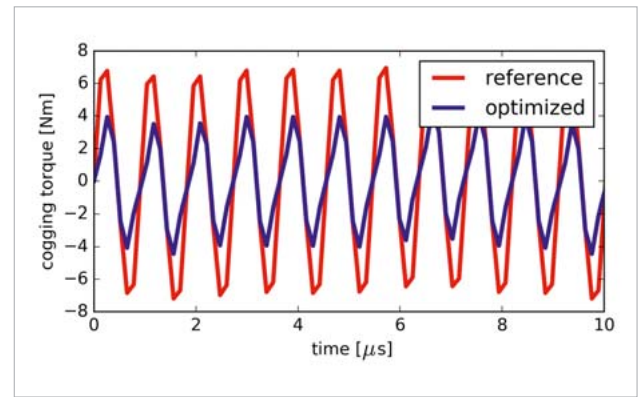


Fig. 5: Cogging torque – comparison of initial versus optimized design

## Conclusion

Electric machine design has always been a challenging task at the multi-physics intersection of electromagnetism, mechanics, and thermal optimization. An economizing problem of allocating space to copper windings, iron and magnets is intertwined with a field shaping problem where many geometry details count. When going from single-working-point motors to demanding dynamic applications, the motor design has to be balanced across a broad range of speeds and loads. The presented IPM motor optimization case study shows that a meta-model-based approach of design understanding and well-targeted optimization is able to reach highly optimized design points at greatly reduced computational cost. MOP-based evolutionary optimization was able to substantially upgrade a successful series production machine.

## Author //

Hayder Al-Khafaji (SIEMENS Large Drives, Nuremberg) /  
Daniel Bachinski-Pinhal (Bundeswehr University Munich) /  
Markus Stokmaier (Dynardo GmbH)

## Source //

[www.dynardo.de/en/library](http://www.dynardo.de/en/library)



## Contact & Distributors

### Worldwide

Dynardo GmbH  
Steubenstraße 25  
99423 Weimar  
Phone: +49 (0)3643 9008-30  
Fax.: +49 (0)3643 9008-39  
www.dynardo.de  
contact@dynardo.de

Dynardo Austria GmbH  
Office Vienna  
Wagenseilgasse 14  
1120 Vienna  
www.dynardo.at  
contact@dynardo.at

### Worldwide distribution of ANSYS optiSLang

ANSYS, Inc.  
Canonsburg  
www.ansys.com

### Worldwide distribution of optiSLang

LightTrans GmbH  
Jena  
www.lighttrans.de

### Germany

CADFEM GmbH  
Grafing b. München  
www.cadfem.de

### Austria

CADFEM (Austria) GmbH  
Vienna  
www.cadfem.at

### Switzerland

CADFEM (Suisse) AG  
Aadorf  
www.cadfem.ch

### Czech Republic, Slovakia, Hungary

SVS FEM s.r.o.  
Brno-Židenice  
www.svsfem.cz

### Sweden, Denmark, Finland, Norway

EDR & Medeso AB  
Västerås  
www.edrmedeso.com

### United Kingdom of Great Britain and Northern Ireland

CADFEM UK CAE Ltd  
Croydon, Surrey  
www.cadfemukandireland.com

### Ireland

CADFEM Ireland Ltd  
Dublin  
www.cadfemukandireland.com

### Turkey

FIGES A.S.  
Istanbul  
www.figes.com.tr

### North Africa

CADFEM Afrique du Nord s.a.r.l.  
Sousse  
www.cadfem-an.com

### Russia

CADFEM CIS  
Moscow  
www.cadfem-cis.ru

### India

CADFEM Engineering Services India  
Hyderabad  
www.cadfem.in

### USA

CADFEM Americas, Inc.  
Farmington Hills, MI  
www.cadfem-americas.com

Ozen Engineering Inc.  
Sunnyvale, CA  
www.ozeninc.com

### USA/Canada

SimuTech Group Inc.  
Rochester, NY  
www.simutechgroup.com

### Japan

TECOSIM Japan Limited  
Saitama  
www.tecosim.co.jp

### Korea

TaeSung S&E Inc.  
Seoul  
www.tsne.co.kr

### China

PERA-CADFEM Consulting Inc.  
Beijing  
www.peraglobal.com

## Publication details

### Publisher

Dynardo GmbH  
Steubenstraße 25  
99423 Weimar  
www.dynardo.de  
contact@dynardo.de

### Executive Editor & Layout

Henning Schwarz  
henning.schwarz@dynardo.de

### Registration

Local court Jena: HRB 111784

### VAT Registration Number

DE 214626029

### Publication

worldwide

### Copyright

© Dynardo GmbH. All rights reserved  
The Dynardo GmbH does not guarantee or warrant accuracy or completeness of the material contained in this publication.